**The Emission and Transport of Volcanic Sulphur Dioxide**

Charlotte Jane Birch

Worcester College
University of Oxford

*A thesis submitted for the degree of*
*Master of Science by Research*

Hilary 2017

# Abstract

Volcanic emissions make an important contribution to the atmospheric sulphur budget. The volcanic contribution of sulphur to the atmosphere is poorly defined due to uncertainties in the amount of sulphur ejected, its distribution by sulphur species and the height of injection. Also there is little or no ground-based monitoring of many volcanoes, and little knowledge of sulphur emitted by degassing and other non-explosive volcanic processes. The altitude of volcanic injections of $SO_2$ is therefore poorly understood, but of great importance when considering the chemistry and movement of the $SO_2$. $SO_2$ reaction rates vary with height and atmospheric composition: $SO_2$ injected into the troposphere will relatively quickly leave the atmosphere as acidification of rainfall; in the stratosphere, however, $SO_2$ is oxidised to $H_2SO_4$, which in aerosol form can remain and affect climate processes for many years. Sulphate aerosols affect the Earth's radiative balance through scattering of sunlight, and are therefore an important factor when considering climate change.

Atmospheric sulphur compounds derive from a variety of sources. The largest direct source of $SO_2$ is from volcanic emission, though it also indirectly stems from conversion from carbonyl sulphide (OCS), the most abundant atmospheric sulphur species.

Satellite-based instrumentation is a vital tool for the analysis of volcanic eruptions. Here the IASI instruments, Fourier transform spectrometers on the MetOp platforms, are used to study medium to large eruptions between 2008-2012. The vertical distribution of $SO_2$ is investigated with respect to the local height of the tropopause, which is then further used to estimate the total atmospheric mass of $SO_2$ as a result of these eruptions. These eruptions are also plotted in terms of their latitude variation, and a large difference between the hemisphere loadings is shown.

The trajectory model HYSPLIT is used in conjunction with the IASI instrument to investigate both the injection height of $SO_2$ plumes and their chemistry. A number of forward trajectories are generated for the duration of the eruption at a series of initial altitudes and the final positions a given time later are compared against the IASI retrieval. It is found that the injection height determined is on average lower than those presented in literature, but that the principle of the analysis is sound. The time frame of the investigation is found to be too short to draw any meaningful conclusions about the plume chemistry.

# The Emission and Transport of Volcanic Sulphur Dioxide


Charlotte Jane Birch

Worcester College

University of Oxford

A thesis submitted for the degree of

*Master of Science by Research*

Hilary 2017

# Acknowledgements

First and foremost I would like to thank Don Grainger for his guidance and support throughout this project: always there to provide a guiding light through the madness, more than anything he taught me that I did know what I was doing, and that however busy everyone may be, there would always be someone to help pull me out of whatever tangled mess I'd created. It was a long and winding road, but we got somewhere in the end.

I would also like to thank the rest of EODG for their collective insight and advise, particularly Elisa for her ever present support and interest, as well as her IASI retrievals, and Anu for his guidance through the early stages of my project. Outside of Oxford, I thank NERC and the Met Office for the funding they provided, and Sandip Dhomse for the model data he shared so willingly, even if that data ended up on the cutting room floor.

Lastly I thank my parents. Without their never-ending support, encouragement and belief this would not have been possible. I owe them everything.

# Abstract

Volcanic emissions make an important contribution to the atmospheric sulphur budget. The volcanic contribution of sulphur to the atmosphere is poorly defined due to uncertainties in the amount of sulphur ejected, its distribution by sulphur species and the height of injection. Also there is little or no ground-based monitoring of many volcanoes, and little knowledge of sulphur emitted by degassing and other non-explosive volcanic processes. The altitude of volcanic injections of $SO_2$ is therefore poorly understood, but of great importance when considering the chemistry and movement of the $SO_2$. $SO_2$ reaction rates vary with height and atmospheric composition: $SO_2$ injected into the troposphere will relatively quickly leave the atmosphere as acidification of rainfall; in the stratosphere, however, $SO_2$ is oxidised to $H_2SO_4$, which in aerosol form can remain and affect climate processes for many years. Sulphate aerosols affect the Earth's radiative balance through scattering of sunlight, and are therefore an important factor when considering climate change.

Atmospheric sulphur compounds derive from a variety of sources. The largest direct source of $SO_2$ is from volcanic emission, though it also indirectly stems from conversion from carbonyl sulphide (OCS), the most abundant atmospheric sulphur species.

Satellite-based instrumentation is a vital tool for the analysis of volcanic eruptions. Here the IASI instruments, Fourier transform spectrometers on the MetOp platforms, are used to study medium to large eruptions between 2008-2012. The vertical distribution of $SO_2$ is investigated with respect to the local height of the tropopause, which is then further used to estimate the total atmospheric mass of $SO_2$ as a result of these eruptions. These eruptions are also plotted in terms of their latitude variation, and a large difference between the hemisphere loadings is shown.

The trajectory model HYSPLIT is used in conjunction with the IASI instrument to investigate both the injection height of $SO_2$ plumes and their chemistry. A number of forward trajectories are generated for the duration of the eruption at a series of initial altitudes and the final positions a given time later are compared against the IASI retrieval. It is found that the injection height determined is on average lower than those presented in literature, but that the principle of the analysis is sound. The time frame of the investigation is found to be too short to draw any meaningful conclusions about the plume chemistry.

# Contents

# List of Figures

# List of Tables

# List of Abbreviations

**Chemical Species:**

**$CS_2$** . . . . . Carbon disulphide

**DMS** . . . . . Dimethyl Sulphide, $CH_3SCH_3$

**$H_2S$** . . . . . Hydrogen sulphide

**$H_2SO_4$** . . . . . Sulphuric acid

**OCS** . . . . . Carbonyl sulphide

**MSA** . . . . . Methane Sulphonic Acid, $CH_3SO_3H$

**$SO_2$** . . . . . Sulphur dioxide

**.** . . . . . .

**IASI** . . . . . Infrared Atmospheric Sounding Interferometer

**ECMWF** . . . European Centre for Medium-range Weather Forecasts

**HYSPLIT** . . Hybrid Single Particle Lagrangian Integrated Trajectory Model

**LIDAR** . . . . LIght Detection And Ranging

**NOAA (ARL)** The National Oceanic and Atmospheric Administration (Air Resources Laboratory)

**OMI** . . . . . Ozone Monitoring Instrument

**RTTOV** . . . . Radiative Transfer model for the Television infrared observation satellite Operational Vertical sounder

**VEI** . . . . . Volcanic Explosivity Index

# 1 Introduction

Sulphur based gases and aerosols are well known and documented to have a huge effect on Earth's climate, through changes to the radiation budget, changes to cloud properties and decreased rainfall, as well as direct effects on human health (Robock, 2000; Schmidt et al., 2012). The $SO_2$ emission from a volcano can also be used to reveal much about its magmatic processes, including relationships between degassing and eruptive style (Oppenheimer et al., 2011). Sulphate aerosols affect Earth's radiation balance, directly through scattering of sunlight (Charlson et al., 1992), and indirectly through modification of the cloud albedo (Twomey, 1977), influencing both radiation and the hydrological cycle (Penner et al., 2001; Stevenson et al., 2003). It is therefore imperative to understand not only the contributions to the atmospheric sulphur budget from volcanoes, but also the altitude at which the gas in injected. This knowledge is also important for air safety (Schmidt et al., 2012). $SO_2$ plumes are often used as a proxy for volcanic ash when forecasting movements of volcanic plumes for the aviation industry, therefore the accuracy of the initial plume altitude reduces the uncertainty in the movement of the plumes, and is clearly more useful as a method of hazard prevention or mitigation.

## 1.1 Current Knowledge of Atmospheric Sulphur

Sulphur is present in many atmospheric trace species, and in both gaseous and aerosol forms. The sources of these species are varied and complex: many come directly or indirectly from volcanic sources, such as sulphur dioxide ($SO_2$), hydrogen sulphide ($H_2S$) and sulphuric acid ($H_2SO_4$), sulphate aerosol; others, such as carbonyl sulphide (OCS) and dimethyl sulphide (DMS, $CH_3SCH_3$), derive from the oceans, from the biological processes of ocean fauna; OCS is also a product of land-based biological processes in soils. Many sources of sulphur are anthropogenic in origin, such as emissions from industry and shipping fuels.

The chemical transfer between these species is governed primarily by photochemical processes, and therefore largely takes place in the stratosphere, above the level of the majority of ozone molecules, which absorb the majority of the photo radiation required for these processes (threshold wavelength for breaking the C-S bond is around 100 nm (Sander et al., 2003)). Most sulphur compounds also react readily with the hydroxyl radical, OH, making their chemical lifetimes very short, on the order of hours, species such as $SO_2$, $CS_2$, OCS and DMS.

Alongside these reactions, other sinks exist for atmospheric sulphur species. Many species are lost through uptake by vegetation, others to wet or dry deposition (Badr and Probert, 1994). $H_2SO_4$ is the most famous species to be lost through acidification of rainfall, however $SO_2$ has also been shown to be lost directly through wet desposition (Chin et al., 2000).

In general, anthropogenic sources of sulphur peak over north America, Europe and south-east Asia, areas of heavy industry, and are larger in the Northern hemisphere, where the greater proportion of land mass facilitates greater industrialisation and settlements. The oceanic sources, on the other hand, such as DMS, peak in the southern hemisphere due to the larger covering of oceans. The plant based processes are much more seasonally dependent, peaking in the summer of the particular hemisphere (Rotstayn and Lohmann, 2002).

By far the biggest contribution to the background levels of sulphur is carbonyl sulphide, OCS. In the troposphere, OCS is a relatively chemically inert species, and

has an approximately constant surface mixing ratio of around 500 pptv, the majority of the loading coming from oceanic emissions, at 0.15 Tg S $yr^{-1}$ (Wayne, 2000). With the exception of OCS, most other sulphur containing species are either too reactive or too soluble to reach the stratosphere by means of atmospheric circulations, and therefore, alongside direct volcanic injection, vertical transport of OCS across the tropopause is the main source of stratospheric $SO_2$. Once transported to the stratosphere, OCS can be broken down by photoinduced processes and ultimately forms $SO_2$, as shown below.

$$\begin{aligned} \mathrm{OCS} + h\nu &\longrightarrow \mathrm{CO} + \mathrm{S} \\ \mathrm{S} + \mathrm{O_2} &\longrightarrow \mathrm{SO} + \mathrm{O} \end{aligned} \qquad \mathrm{O} + \mathrm{OCS} \longrightarrow \mathrm{SO} + \mathrm{CO}$$

$$\begin{aligned} \mathrm{SO} + \mathrm{O_2} &\longrightarrow \mathrm{SO_2} + \mathrm{O} \\ \mathrm{SO} + \mathrm{O_3} &\longrightarrow \mathrm{SO_2} + \mathrm{O_2} \end{aligned}$$

Sheng et al. (2015) report that the photodissociation pathway accounts for about 80 % of the conversion between OCS and $SO_2$, but Chin and Davis (1995) state that OCS is unlikely to be responsible for any measurable increase in the levels of stratospheric aerosols, due to the measured concentrations being fairly stable during the 15 years preceding the study (Chin and Davis, 1993). From these stable concentrations, it was clear that the global sources of OCS were almost entirely balanced by the global sinks, and from dividing their estimate of the total mass of OCS in the atmosphere by the source strength, Chin and Davis (1995) estimate the OCS lifetime to be 4.3 years. It is this long lifetime which means that it is the only tropospheric sulphur species to be transported above the tropopause (Badr and Probert, 1994).

The seasonal variation of OCS has been used by Montzka et al. (2007) as a proxy for studying global sulphur. Through use of multiple ground-based and airborne measurements, they report the highest annual mean mixing ratios of OCS to occur nearest the equator. This variability suggests stronger sources, or weaker sinks, nearer the equator, which in turn could suggest an enhanced photooxidation of $CS_2$ and of DMS complexes, both of which have OCS as a primary product. They also

note that whilst a seasonal variation is evident in both the northern and the southern hemispheres, it arises from different processes: in the southern hemisphere, the variation is driven by the flux of OCS and its precursors from the oceans, whereas in the northern it arises from enhanced uptake by vegetation during the growing season. The rate of OCS crossing the tropopause due to upwelling in the tropics was calculated by Chin and Davis (1993) to be 0.64 Tg $yr^{-1}$. While $CS_2$ is far less abundant, and with highly variable concentrations usually between 2-120 ppt and a lifetime on the order of a few weeks, tropospheric oxidation processes produce OCS.

The lifetime of sulphur dioxide molecules in the troposphere is on the order of a few days (Wayne, 2000). The amount is highly variable, above a low background concentration, dependant on such factors as volcanic activity and the proximity of industry. Clean continental air contains less than 1 ppb of sulphur dioxide, corresponding to a total column density of $< 0.2$ DU in a boundary layer of 2 km (Eisinger and Burrows, 1998). It is removed from the troposphere by formation of sulphuric acid, both by aerosol absorption and by forming condensation nuclei for aerosols and clouds. The lifetime of sulphur dioxide molecules in the stratosphere is several weeks, during which time sulphate aerosols are also formed.

The atmospheric reactions of $SO_2$ are very complex, and proceed through three different pathways to the sulphate ion ($SO_4^{2-}$): through reaction with the hydroxyl radical (OH) to form an $HSO_3$, which can react in turn with either another hydroxyl radical to form water and $SO_3$ or just $H_2SO_4$, or with oxygen to form $SO_3$ followed by a further reaction with water (as shown below); through dissolving in water droplets where it can react with oxygen gas to form $SO_4^{2-}$; and finally through reaction with hydrogen peroxide. The ultimate fate of all sulphur in the atmosphere is to be oxidised to the sulphate ion, usually as sulphuric acid, $H_2SO_4$.

$$SO_2 + OH \xrightarrow{M} HOSO_2$$

$$HOSO_2 + O_2 \longrightarrow HO_2 + SO_3$$

$$SO_3 + H_2O \xrightarrow{M} H_2SO_4$$

Or alternatively:

$$SO_2 + OH \longrightarrow HOSO_2$$
$$HOSO_2 + OH \longrightarrow H_2O + SO_3$$
$$HOSO_2 + OH \longrightarrow H_2SO_4$$

$SO_2$ is converted to $H_2SO_4$ in the stratosphere with an e-folding time of 1 month (Wayne, 2000). The $H_2SO_4$ vapour is then converted to liquid. This is either by combination with $H_2O$ to form $H_2SO_4.nH_2O$ complexes, or by condensation onto pre-existing particles of radius greater than 0.15 microns (µm), such as dust from the surface or meteoric matter.

Volcanic aerosols reflect short-wave solar radiation and absorb long-wave terrestrial radiation. Stratospheric volcanic aerosols can persist for several years since there is no wet deposition in the stratosphere, and particle fall speeds are very low. They must, therefore, settle into the troposphere by dry deposition before they can be removed. The sulphate layer at approximately 30 km (the Junge layer) is enhanced by volcanic eruptions, which can cause depletion of stratospheric ozone, since sulphate aerosols can act as a surface on which chlorine activated ozone depletion can occur.

In general, the chemistry of inorganic sulphur containing species in driven by the hydroxyl radical:

$$OH + CS_2 \longrightarrow COS + SH$$
$$OH + COS \longrightarrow CO_2 + SH$$
$$OH + H_2S \longrightarrow H_2O + SH$$

In the presence of $O_2$, $O_3$ or $NO_2$, the SH radicals are oxidised further to $SO_2$, via SO, HSO or S intermediate species.

Source strengths and atmospheric concentrations are related by the atmospheric lifetimes, which in turn is closely linked to the reactivity. For instance, OCS has the largest burden, roughly 15 times that of $SO_2$ in places, and yet it has a source flux of around 100 times less. This implies an OCS tropospheric lifetime around

1500 times longer than that of $SO_2$. Current estimates of the lifetime of OCS is on the order of 4 years (Chin and Davis, 1995), while $SO_2$ is removed in about a day by dry deposition and a week by gas-phase chemistry, so this estimated value of OCS lifetime being 1500 times longer than that of $SO_2$ is a sensible order of magnitude. Table 1.1 illustrates the relative quantities of the major atmospheric sulphur species, as well as the various sources and sinks. The fluxes and burdens of these species can be seen in figure 1.1.

### 1.1.1 Chemistry of the Stratosphere vs. Troposphere

There exists significantly different chemical dynamics between the stratosphere and the troposphere. Reactions requiring particular wavelengths of radiation to initiate will only occur in the stratosphere, above the highly absorbing ozone layer. Conversely reactions requiring a third molecule, such as those detailed in the sulphate formation reaction scheme in Section 1.1, occur at a much slower rate in the stratosphere, due to the low concentration of molecules: when there are so few molecules present, a two party collision is unlikely enough, but a three body is proportionally even more improbable.

A good example of the first case is $SO_2$. $SO_2$ cannot be photodissociated in the troposphere because the S-O bond requires a wavelength of around 210 nm to break. This wavelength does not penetrate the ozone layer to reach the troposphere, so photodissociation does not play a part in the chemistry here. However, radiation can be absorbed to form the excited singlet and triplet states in the stratosphere.

**Table 1.1:** The quantities, sources and sinks of the most abundant atmospheric sulphur species

| Species | Quantities | Sources | Sinks |
|---|---|---|---|
| **OCS** | 500 pptv (Chin and Davis, 1995)<br>Uniform across troposphere, stratosphere higher in the tropics | Troposphere: Oxidation of $CS_2$, volcanoes, oceans, biomass burning, shipping fuel<br>Stratosphere: Volcanoes, tropical upwelling (Eyring et al., 2010) | Reaction with O and OH radicals, photolysis, vegetation uptake, land uptake, downwelling during polar winters |
| **$SO_2$** | Background troposphere, 20 pptv to 1 ppbv | Troposphere: Volcanoes, industry<br>Stratosphere: Conversion from OCS, volcanoes, upwelling in tropics | Oxidation by OH radicals to $H_2SO_4$, downwelling during polar winters, photolysed in spring |
| **$H_2SO_4$** | Uncertain | Gaseous: oxidation of $SO_2$ in the stratosphere<br>Aerosol: spontaneous clustering of $H_2SO_4$-$H_2O$ complex, or around a nucleus | Deposition of aerosol form |
| **$CS_2$** | 2-200 pptv | Volcanoes | Reaction with OH radical and photolysis |
| **$H_2S$** | Remote ocean: 5-15 pptv<br>Coastal waters: 100-300pptv<br>Land: 5–150 pptv<br>Near industry: 1-100 ppbv | Anaerobic soils, plants, paper manufacture (troposphere) and volcanoes (troposphere, some stratosphere) | Reaction with OH radical |
| **DMS** | Average near-surface mixing ratios over:<br>Oceans: 100 pptv<br>Land: 20 pptv | Marsh land (bacteria) Ocean phytoplankton (troposphere only) | Chemically: hydroxyl radical abstraction and addition |

Quantities data taken from Jacobson (2005) unless otherwise stated.

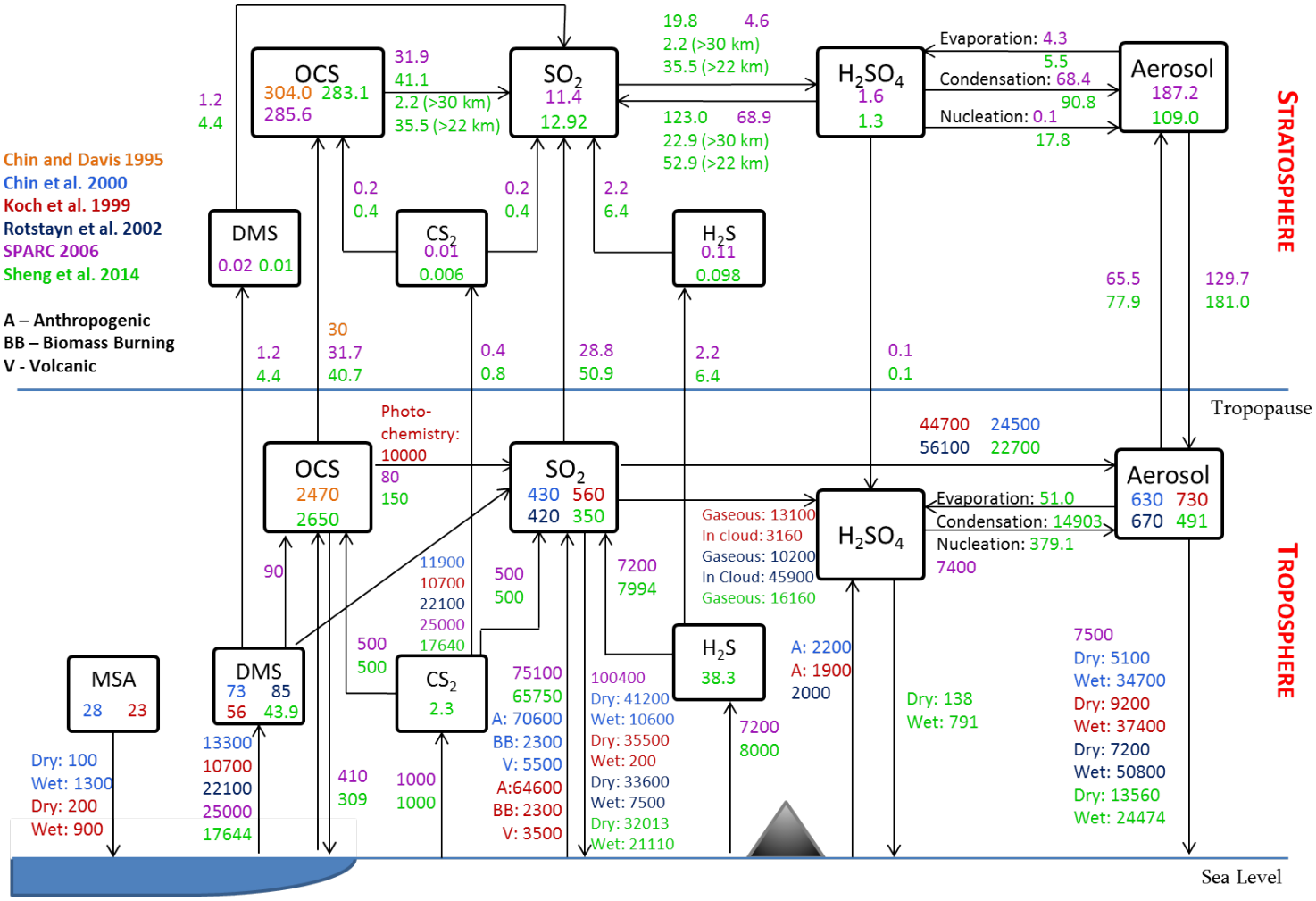


**Figure 1.1:** A representation of the global atmospheric sulphur budget. Species and atmospheric burdens are shown in the boxes, in units of Gg S. Net fluxes are represented by the arrows, pointing in the direction of net flow unless otherwise indicated, and values in units of Gg S $yr^{-1}$. Values are taken from various atmospheric models: GOCART, Chin et al. (2000), in light blue; GISS, Koch et al. (1999), in red; CSIRO, Rotstayn and Lohmann (2002), in dark blue; SOCOL-AER, from the 2006 SPARC report (Thomason and Peter (2006) in purple and Sheng et al. (2014) in green); and from measurements, Chin and Davis (1995), in orange.

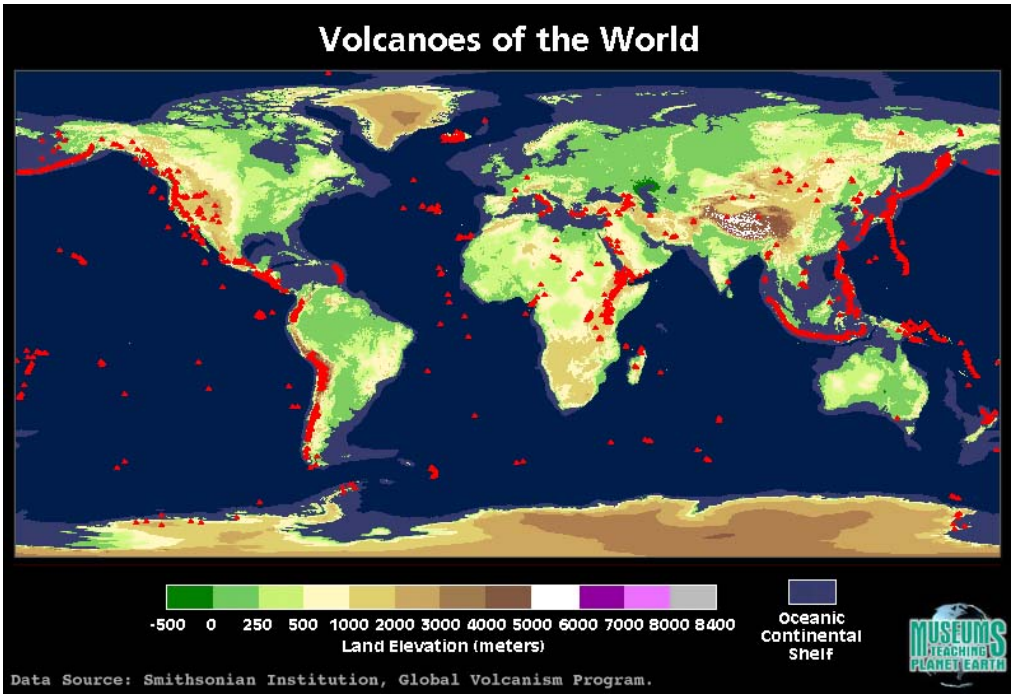


**Figure 1.2:** Map of the locations of known volcanoes, as recorded by the Smithsonian Institution, Global Volcanism Program. Image reproduced from Prentiss (2015)

### 1.1.2 Scale of Volcanic Eruptions

The scale of a volcanic eruption is important in determining its climactic importance: the eruption magnitude determines whether or not the volcanic products are injected into the stratosphere in large quantities. A large explosive eruption, such as that of Pinatubo in 1991, may result in a direct stratospheric injection of $SO_2$, whereas products from a smaller eruption or passive degassing may never leave the troposphere at all. The location is also important: when volcanoes situated in the tropics erupt, the erupted material from even the smaller eruptions have a good chance of reaching the stratosphere, due to being lofted by atmospheric circulations, and a high proportion of volcanoes are situated in the mid latitudes. A representation of the locations of all known volcanoes is shown by the red triangles in figure 1.2. As can be seen, there are clusters of volcanoes around Indonesia and eastern Africa, though they are spread fairly regularly around the Pacific Ocean.

The current knowledge of quiescent volcanism is very poorly constrained. This is partly due to the remote location of many volcanoes: without any permanent

nearby habitation, it is significantly more difficult to take long term measurements. In addition, most quiescent degassing happens low down in the troposphere, below the operational limit of most satellite observations. The contribution of quiescent volcanism to the annual sulphur budget is extremely uncertain (Carn et al., 2013).

The majority of monitoring of passive degassing takes place on a volcano by volcano basis, by ground based instrumentation around, for example, fumeroles (Mather et al., 2008). However, these datasets are extremely limited, and based on the accessibility of the volcanoes, and the short lifetime of the experiments themselves. Sparks et al. (2012) state that as much as 90% of active volcanoes are only minimally monitored, or have no monitoring at all. One of the most important advances in the study of passive volcanic degassing was the launch of the Ozone Monitoring Instrument (OMI), flying aboard NASA's Aura satellite in 2004 and measuring in the shortwave region with reflectance spectrometry. OMI it is particularly useful for imaging the lower troposphere where the majority of atmospheric species are situated, in contrast to an instrument like IASI, which struggles to image low altitudes due to the degree of thermal contrast between the atmosphere and the ground. In fact, it is possible to measure emissions as low as 30 kt $yr^{-1}$ with OMI (Fioletov et al., 2011), making it an ideal instrument for the observation of low emission sources, like degassing volcanoes. Symonds et al. (2001) suggest that an emission rate of greater than 100 t $day^{-1}$ of $SO_2$ should be regarded as indicative of magma intrusion, and could perhaps be a precursor to an eruption, therefore the capability of OMI to image down to this level means a great advance in the field of near real time volcano monitoring. Carn et al. (2013) approximate threshold daily detection of $SO_2$ by OMI to be around 1000 t $day^{-1}$, and recognise that this value is similar to that suggested by Werner et al. (2011) as the threshold $SO_2$ emission in Alaska leading to an eruption. OMI does, however, have some drawbacks: relying on reflected UV radiation means that it can only image during the day, potentially missing large amounts of injection. The retrieval of $SO_2$ also has a lot of interference from ozone, the species the instrument is designed to detect, which is where an instrument such as IASI has an advantage, using a combination

of absorption bands in it's detection (see chapter 2). It is therefore evident that for OMI $SO_2$ data to be useful for gauging the likelihood of eruption, it should be used alongside other observations (Moran et al., 2011).

Schmidt et al. (2012) investigate the contribution of these passive degassing events to the global level of background aerosols. They use a global aerosol microphysics model to quantify the impact of the emissions on the cloud albedo radiative forcing, under both pre-industrial and present-day conditions. They find that passive volcanic degassing increases global annual mean cloud droplet number concentrations by 40 % under the pre industrial conditions, but only 10 % under the simulated present day. They seek to explain this phenomena by stating that a lower background aerosol level means less volcanic aerosols are formed on emission, as there are less condensation centres for the aerosols to form around, and that more aerosols are formed per unit of volcanic sulphur emission in the pre industrial era.

As well as imaging the lower tropospheric process, OMI has also been used to study larger eruptions. Since 2004, OMI has detected $SO_2$ plumes from eruptions of over 30 volcanoes (McCormick et al., 2013). These eruptions cover a wide range of geographical locations and of $SO_2$ emission concentrations. These small eruptions (Volcanic Explosivity Index of 4 or less) are of particular interest as the higher levels of atmospheric water vapour at lower altitudes interferes with the retrievals of IR instruments, such as IASI. Eruptions detected by OMI that have low to moderate $SO_2$ release or lower altitude plumes include Merapi (2010) in Indonesia, Eyjafjallajökull (2010) and Grìmsvötn (2011) in Iceland, and Puyehue (2011) and Llaima (2008), both in Chile. OMI has also detected small and short-lived eruptions from volcanoes with little prior evidence of activity, for example the 2006 eruption of Fourpeaked in Alaska (Carn et al., 2013).

## 1.2 Ongoing Questions

Retrieving the height of injection of volcanic eruptions is a largely poorly understood area of study. A nadir scanning satellite will have an inherent difficulty with retrieving plume heights due to their top-down perspective. Ground based and

in situ measurements, such as LIDAR stations or balloon borne instruments, rely on a local presence at the site of the eruption, and although they would give a great insight into the injection height of the plume, with so few volcanoes actively monitored this is an unlikely outcome (Sparks et al. (2012) state that as much as 90% of active volcanoes are only minimally monitored, or have no monitoring at all). Satellite retrievals have had some success in recent years with estimating the height (Eckhardt et al. (2008), Yang et al. (2009) and similar). In particular the algorithm of Carboni et al. (2012), which uses optimal estimation to compare the observed spectra with those from a range of simulated eruptions, is yet to be exploited to investigate the long term distribution of erupted $SO_2$ amount and altitude. Eckhardt et al. (2008) use a similar method comparing simulated spectra with observations to minimise error, but instead of simulating atmospheric conditions and constituents, they use an atmospheric transport model (FLEXPART) to exploit the fact that winds change with altitude, and therefore the position and shape of the plume contain information on its altitude, as it is perturbed by the wind. Their method was found to be very computationally fast, and therefore useful for aviation and other hazard warnings, and was very successful at estimating injection altitudes for the middle to upper troposphere.

With respect to atmospheric sulphur burdens and fluxes, the troposphere is relatively well described, being the simpler of the regions to model. However there is a general discrepancy between modelled data sets. Models focusing on the stratosphere tend to massively over simplify tropospheric processes (Thomason and Peter (2006), chapter 6) whereas others will take great care in estimating all known tropospheric phenomena (Chin et al., 2000). There still remains a significant uncertainty in these values.

Evidence for the seasonal variability of sulphur burdens, other than OCS, seems rather poorly investigated. However, much can be inferred from knowledge of the sources and sinks: $SO_2$ is also transported across the tropopause in the tropics, and back down over the poles during the polar winter, so a peak in tropospheric $SO_2$ should be observed in the winter hemisphere. Due to the oxidation of OCS to

$SO_2$, and further to $H_2SO_4$, a corresponding stratospheric seasonal trend should also be seen in these species. To investigate the validity in these claims through satellite measurements would therefore be a worthwhile field of study.

Rex et al. (2014) report on how their observations of a pronounced minimum in the tropospheric column of ozone over the West Pacific has a direct effect on the global sulphur budget, through ozone sonde measurements, verified with a chemistry and transport model. Due to the uprising of warm air, the West Pacific warm pool is the main source of stratospheric air, and therefore any changes in tropospheric composition in this region have a major impact on the stratospheric composition. They suggest that the lack of ozone in this region directly corresponds to a minimum in OH, which in turn increases the concentration of $SO_2$, as OH is a major sink for stratospheric $SO_2$. Therefore, any $SO_2$ from volcanic eruptions or anthropogenic sources has a much longer lifetime in this region. Since the OH minimum facilitates the transport of $SO_2$ across the tropopause, the sulphur emissions from smaller, tropospheric injections are able to reach the stratosphere, which under normal circumstances would be confined to the troposphere, and can therefore have significantly more impact on climate. Results from Rex et al. (2014) seem to confirm the premise but satellite verification would be required to confirm the process outright.

## 1.3 Questions Arising

The aim of this project is to quantify the $SO_2$ emitted globally from volcanoes each year, from both explosive events and quiescent volcanism, and to assess how these emissions vary over time.

- Can IASI be used to verify the $SO_2$ loading above and below the tropopause presented in figure 1.1? What do the emission profiles look like when presented as a function of the local tropopause height? What information can this provide on latitudinal variation, relative plume altitudes and relative $SO_2$ concentration?

- Can plume trajectories be used to estimate the injection altitude of a parcel of $SO_2$? Can the trajectories be used to create a forward model to use in conjunction with IASI, and can this be extended to measure chemical rates of change within a plume?

# 2
# Instrumentation

Atmospheric sulphur dioxide has been measured by a variety of different satellites, and by a range of different methods, over the past decade. Instruments such as the Ozone Monitoring Instrument (OMI, Carn et al. (2008)) and the Microwave Limb Sounder (MLS, Read et al. (1993)) aboard NASA's Aura satellite, measuring the the nadir and limb respectively, The Atmospheric InfraRed Sounder (AIRS, Carn et al. (2005)) aboard NASA's Aqua satellite and the Ozone Mapping Profiler Suite (OMPS, Yang et al. (2013) have all provided insights into the transport and chemistry of $SO_2$ in the troposphere.

Satellite remote sensing has many advantages over ground-based or balloon measurements: data can be gathered over a long period of time, and in the case of orbiters, over a much larger area than any ground-based counterparts; multiple sensors may be mounted on the same platform, allowing for a greater range of spectral coverage of the same areas. Although such methods as airborne imaging result in a much greater spatial resolution, the range of these flights in extremely limited, and multiple flights are often cost prohibitive. There is also the problem of the safety of the aircraft itself, to take measurements of a volcanic plume would require many instruments to be flown directly through the plume, thus risking damage to the aircraft's engines. Satellite instrumentation has no such problems, and is also able to image remote areas where ground-based instruments such as LIDAR

cannot be operated. There are, however, some drawbacks to the use of satellite remote sensing, alongside the lesser spatial and temporal resolution. Although the cost compared to the amount of data which can be collected is relatively cost efficient, the initial cost of developing the equipment and getting a satellite into orbit is incredibly high. As well as the on-going costs of monitoring and analysing the data received, if anything were to malfunction or become damaged on the satellite, little can be done from the ground to remedy it. Aside from cost, most satellite based spectrometers and radiometers still have problems with cloud cover, along side their individual operational limits of spatial resolution.

Satellite imaging alone does not give a complete picture of the atmosphere. In fact, nadir and limb scanning instruments working together, often in conjunction with ground-based LIDARs, for example, can paint a much clearer picture of atmospheric processes than might otherwise be available individually.

## 2.1 IASI

The Infrared Atmospheric Sounding Interferometer (IASI) is a nadir viewing Fourier transform spectrometer flying aboard the MetOp series of polar-orbiting satellites, the first of which, MetOp-A, was launched in 2006, with MetOp-B following in 2012, and MetOp-C planned for a 2017 launch.

The Fourier Transform infrared spectrometers aboard the IASI instruments use the signal emitted from the Earth, and detects how it is absorbed and scattered by the atmosphere and the trace gases it contains. A schematic for a standard Fourier Transform Interferometer is shown in figure 2.1. The incoming radiation from the atmosphere is split into two parts by a beam splitter, meaning that half will follow path 1 to the detector and half path 2 causing the two beams to interfere with each other when they recombine. The difference in these two paths is the optical path difference (OPD), and an interferogram is obtained by varying the OPD and recording the intensity at the detector, ranging from completely constructive (bright) to completely destructive (dark) interference. For polychromatic light, the interferogram will be the sum of the monochromatic interferograms at all

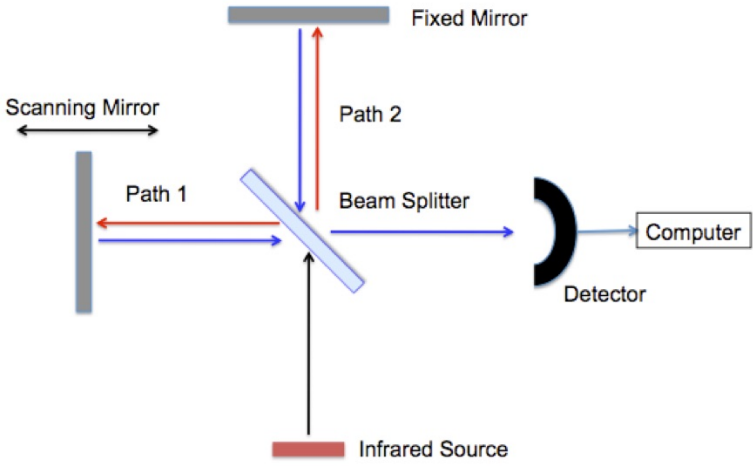


**Figure 2.1:** Schematic of a Fourier Transform Interferometer, reproduced from Soucy et al. (2006)

frequencies, and the spectrum of incoming radiance is generated from the inverse Fourier transform of the interferogram.

The IASI instruments operate in the 3.7 - 15.5 µm (645 - 2760 $cm^{-1}$) spectral range and provide full global coverage four times per day, over 14 orbits each in sun-synchronous motion. Data is collected in 2000 km wide swaths, and each field of view has a horizontal resolution of 50 x 50 km, comprising of four 12 km diameter circular pixels in a 2 x 2 grid (figure 2.2). The full technical specifications of IASI can be found in Blumstein et al. (2004), and the objective of the MetOp mission was to provide continuous and long-term data, for use in meteorology and climate monitoring (Clerbaux et al., 2009).

The $\nu_1$ (symmetric stretch), $\nu_3$ (asymmetric stretch) and $\nu_1 + \nu_3$ (combination band) absorption bands of $SO_2$ lie centred around 8.7, 7.3 and 4 µm respectively, making IASI an ideal instrument for the study of atmospheric $SO_2$, though the individual bands are useful for different spectroscopic applications. The $\nu_1 + \nu_3$ band is weakest, and often drowned out during the day by reflected solar radiation, but it becomes useful at high $SO_2$ concentrations when the other bands can become saturated (Karagulian et al., 2010). The $\nu_3$ asymmetric stretching band has the strongest absorption, but coincides with the water absorption limiting its usefulness, particularly at low altitudes. It is, however, still the used by Clarisse et al. (2010)

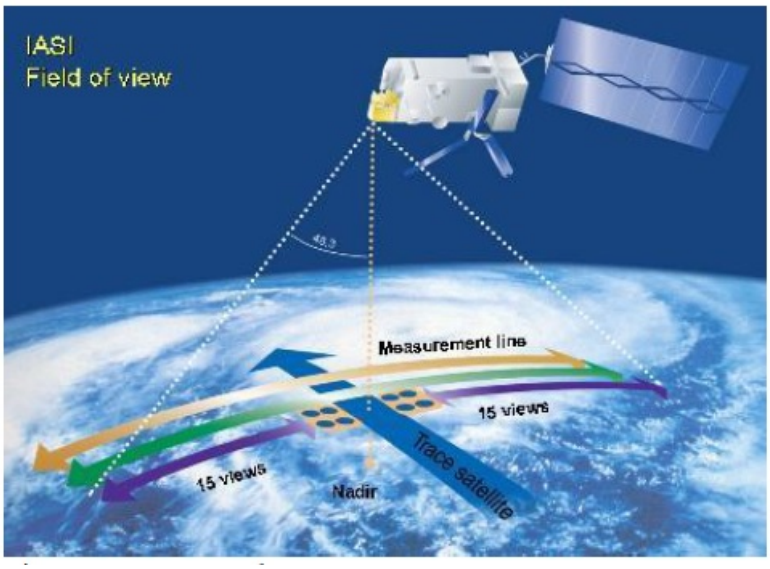


**Figure 2.2:** IASI ground coverage, showing the 30 views which comprise each scan, and the 2x2 grid of circular pixels making up the individual views. Image reproduced from Blumstein et al. (2004)

for their retrievals using an assumed altitude, Clarisse et al. (2014) to retrieve altitude alone, and by ESA's Support to Aviation Control Service (SACS) for the near real-time $SO_2$ flagging (Brenot et al., 2014). The $\nu_1$ symmetric stretching band, which is used in combination with the $\nu_3$ band in Carboni et al. (2012) and the data used in this work, is used to provide some insight into the lower troposphere.

The retrieval algorithm developed at the University of Oxford by Carboni et al. (2012) uses both the $\nu_1$ and the $\nu_3$ band: both bands are sensitive to the altitude of the plume and its $SO_2$ concentration, as illustrated in figure 2.3. The absorption of both bands is reduced by other atmospheric constituents, so an increase in the altitude of the plume produces a stronger $SO_2$ absorption, as does increasing the $SO_2$ concentration. It is worth noting that the $\nu_1$ signal does not change significantly in spectral shape between plumes at different altitudes, whereas the $\nu_3$ band does. The change in the shape of the $\nu_3$ absorption band is caused by the absorption of other gases, such as water vapour, which are more concentrated lower in the atmosphere. It is, therefore, this part of the spectrum that contains information on the plume altitude. It is also therefore vital to use the correct altitude in the retrieval in order to get an accurate amount of $SO_2$.

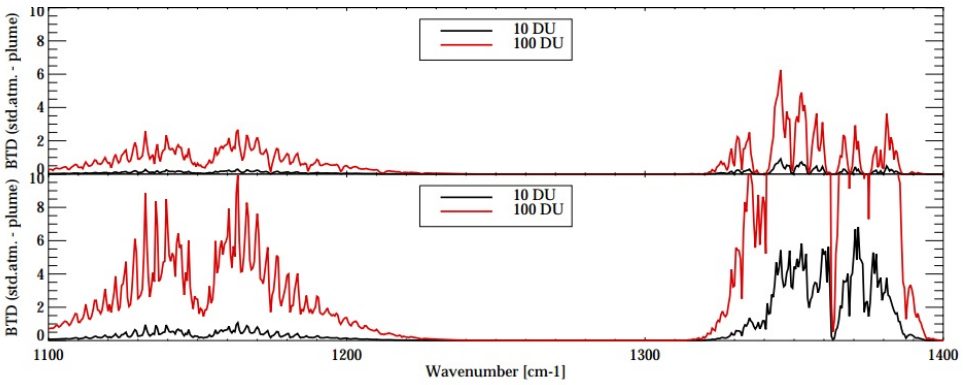


**Figure 2.3:** Simulated IASI brightness temperature spectra for, Top: the brightness temperature differences ($\Delta T_B$) between the reference clean atmosphere and the same atmosphere enhanced by a tropospheric $SO_2$ plume; Bottom: $\Delta T_B$ between the reference clean atmosphere and the same atmosphere enhanced by a stratospheric $SO_2$ plume; both containing a total column amount of 10 DU(black line) and 100 DU (red line) of $SO_2$. Figure adapted from Carboni et al. (2012)

The IASI retrieval algorithm described in Carboni et al. (2012) is summarised in figure 2.4. It assumes a Gaussian $SO_2$ profile, with the $SO_2$ confined to one single plume: the $SO_2$ column amount, the spread and altitude of the profile and the surface temperature are estimated for each pixel through an optimal estimation retrieval (Rogers, 2000). A forward modelled spectra for a clean atmosphere under certain atmospheric conditions, as defined by ECMWF[1] atmospheric profiles, is generated, to which the modelled contribution of a plume is added. The best fit between the IASI measurements and the forward model brightness temperature spectra, modelled using RTTOV[2], is found using optimal estimation (Rogers, 2000). A range of modelled spectra are matched against the observations, with the aim of minimising the cost function, which is defined as a specific combination of the clean atmospheric state, the state of the $SO_2$ plume, the error associated with those states, the measurements and any a priori assumptions about the plume (when there is not enough $SO_2$ to retrieve the plume altitude, for example), so the $SO_2$ concentration and height retrieved will be the input of these to the forward model which give the minimum cost function. When the measurements contain a particularly low

[1]The European Centre for Medium-Range Weather Forecasts, ECMWF
[2]Radiative Transfer for TOVS, `http://nwpsaf.eu/deliverables/rtm/rttov_description.html`


**Figure 2.4:** A visualisation of the retrieval algorithm described in Carboni et al. (2012), adapted from Preston (2015). The retrieval seeks to minimise the cost function, ***J'***, for each pixel via optimal estimation. The output of the retrieval represents the $SO_2$ conditions in the forward model which best fit the observed spectra

amount of information, the output from the retrieval will be strongly influence by the a priori values, so the "first guess" is of vital importance.

Despite the combination of spectral bands, IASI does sometimes struggle to image lower down in the troposphere. This is due to the nature of the measurements, relying on the thermal contrast between the hot ground and the cold atmosphere. Too close to the ground, the temperatures start to equalise and the measurements become indistinguishable from the noise. An alternative would be to measure reflectance spectra, which are the most sensitive down in the lower troposphere, but these fall down when gas concentrations become too low, at higher altitudes, and also close to low reflectivity surfaces such as oceans. The two methods are, however, complimentary and are useful when used in combination.

### 2.1.1 Oxford Archive

The Earth Observation Data Group at the University of Oxford stores and maintains an archive of $SO_2$ retrievals from the lifetime of the IASI instrument (Carboni et al., 2016). The archive is limited to the geographical region around volcanic eruptions with plumes of sufficient altitude and $SO_2$ concentration to register above the background in a linear retrieval. A summary of the eruptions investigated is shown in Table 2.1, and includes a brief description or comment about the eruption.

**Table 2.1:** A table listing the archived eruptions retrieved by IASI A

| Volcano | Dates Retrieved | Box Retrieved[A] | Comment[B] |
|---|---|---|---|
| **2008** | | | |
| Llaima | 2 - 6 Jan | 20 - 55°S<br>All Longitudes | VEI 3, small Strombolian eruption. Plume only connected to the volcano on the first day, and confined to the troposphere |
| Okmok | 12 - 20 July | 60 - 30°N<br>180 - 60°W | VEI 4, explosive eruption. $SO_2$ injected around tropopause and spreads south and east. Plume altitude increases with time following the tropopause |
| Kasatochi | 7 - 22 Aug | 90 - 30°N<br>All Longitudes | VEI 4, explosive eruption. Continuous injection of $SO_2$ up to tropopause and stratosphere, concentration at a maximum after 7 days. After 10 days, presence of $SO_2$ at all latitudes between 30 and 90°N |
| Dalaffilla | 4 - 7 Nov | 60°N - 10°S<br>10°W - 145°E | VEI 3, effusive eruption. Plume is divided into two parts: lower in troposphere, and higher tropopause/stratosphere. $SO_2$ near the volcano in every image indicates continuous emission |
| **2009** | | | |
| Sarychev | 11 - 26 June | 90 - 30°N<br>All Longitudes | VEI 4. Initial small tropospheric plume building up with increasing $SO_2$ load, maximum on 16 June and reaching tropopause and stratosphere |
| **2010** | | | |
| Nyamuragira | 3 - 12 Jan | 20°N - 20°S<br>10 - 50°E | VEI 1, flank fissure eruption. Began on 2 Jan 2010, and continued intermittently for 3–4 weeks, confined to the troposphere |
| Soufrière Hills | 10 - 15 Feb | 40°N - 10°S<br>100 - 20°W | VEI 3, large dome collapse. Plume was divided into two parts: a higher one around 16– 19 km (tropopause/stratosphere) and a lower one in the troposphere. The lower plume undetectable after 1 day, while the higher one spread east, south east |

[A] Approximate latitude / longitude area retrieved
[B] Adapted from Carboni et al. (2016) and Venzke (2013)

**Table 2.1:** Continued

| Volcano | Dates Retrieved | Box Retrieved | Comment |
|---|---|---|---|
| Merapi | 4 - 11 Nov | 10°N - 40°S<br>60 - 150°E | VEI 4, major explosive eruption. High plume, up to tropopause and stratosphere, but issues with an old plume passing over |
| **2011** | | | |
| Grìmsvötn | 21 - 26 May | 80 - 45°N<br>50°W - 40°E | VEI 4, strong explosive eruption. Higher part of the plume moved west and north reaching the tropopause/stratosphere. The lower part travelled south towards Europe and was confined to the troposphere |
| Puyehue | 5 - 30 June | 20 - 60°S<br>All Longitudes | VEI 5, major sequence of explosive and effusive eruptions. The plume reached the tropopause/stratosphere and can be followed traveling around the Southern Hemisphere 3 times in 30 days |
| Nabro | 12 - 24 June | 60°N - 10°S<br>10°W - 150°E | VEI 4. The highest emission of SO2 for the period considered (2008–2012). Two plumes were detected at different altitudes, the highest one reached the stratosphere, the lower remained confined to the troposphere |
| Nyiragongo | 7 - 15 Nov | 20°N - 20°S<br>10 - 50°E | VEI 2, major flank fissure eruption. Began with fire fountains and a long lava flow. Emissions confined to the troposphere |
| **2012** | | | |
| Copahue | 22- 27 Dec | 20 - 60°S<br>All Longitudes | VEI 2, moderate explosive eruptions. The plume can be seen to be connected with volcano every day, and was confined to the troposphere |

# 3

# Explosive Eruptions at the Tropopause

Of the eruptions that occur every year, most only result in a tropospheric injection of sulphur species. Although this certainly contributes to the atmospheric loading of sulphur, it is the stratospheric injections which lead to the huge increases in the levels of aerosol, and so the changes to climate: Sheng et al. (2014) report that a small to moderate eruption such as that of Nabro in 2011, may as much as double the stratospheric aerosol loading. In fact, earth has not seen a large stratospheric injection of sulphur since the eruption of Pinatubo in 1991, though Vernier et al. (2011) report a systematic increase in stratospheric aerosol levels, which they have attributed to a series of moderate but increasingly intense eruptions in the mid latitudes, injecting sulphur at 18 to 20 km, which was then transported into the stratosphere by atmospheric circulations.

One eruption in particular in recent years has sparked debate, on the matter of whether or not it was a stratospheric injection of $SO_2$ is that of Nabro, in 2011. Clarisse et al. (2014) retrieved altitudes of initial $SO_2$ injection of between 15 and 17 km, from where they suggest the $SO_2$ was then entrained in the Asian monsoon anticyclone, which transported the $SO_2$ across the tropopause, which they measure to be at 16 to 18 km in altitude. Once it crossed the tropopause, Clarisse et al. (2014) observed the $SO_2$ ascend slowly through the stratosphere, spreading as it went. So although some $SO_2$ may have been injected directly into the stratosphere,

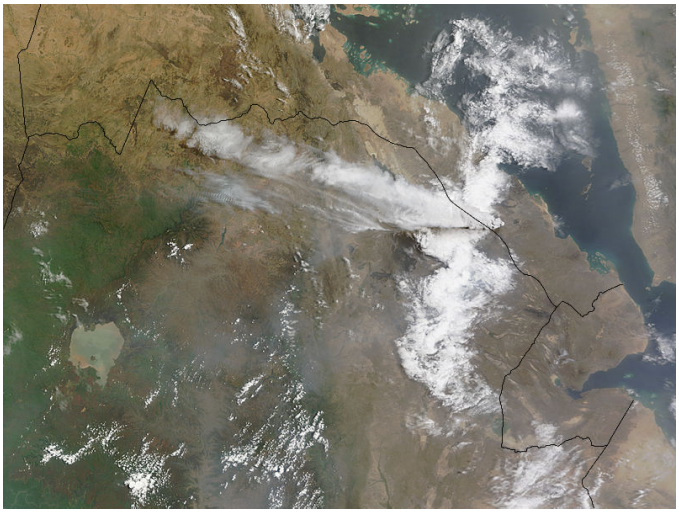

**Figure 3.1:** Image of the plume from Nabro, captured by terra/MODIS at 08:15 UTC on the 16th June 2011; the plume can clearly be seen to be above the clouds.

some also entered via the monsoon anticyclone circulation, but by either mechanism, the majority of the $SO_2$ from the Nabro eruption seems to have moved into the stratosphere. This assertion is refuted by Fromm et al. (2014), who state that the anticyclone circulation is not needed to explain the presence of $SO_2$ in the stratosphere, that it was merely injected at the tropopause height.

## 3.1 Loading at the Tropopause

The aim of the work in this section is to plot the $SO_2$ erupted from any given volcano, as measured by IASI, as a function of the height of the tropopause at that latitude, with the aim of resolving the amount of $SO_2$ directly injected into the stratosphere compared to that injected into the troposphere.

In general when plotting the vertical extent of a volcanic plume, the "amount" of $SO_2$ is simply plotted against the altitude at which it was retrieved (figure 3.2a), or alternatively, the total column amount is taken to be the peak of a Gaussian with some assumed vertical spread $\sigma$ (figure 3.2b), the total mass of sulphur emitted being calculable by the area under the curve in both cases. The issue with this way of representing the data in this case can also be seen in the figure (3.2c), as when the altitude of the plume is plotted against its latitude with the height of the tropopause, clearly two plumes at the same altitude but different latitudes will

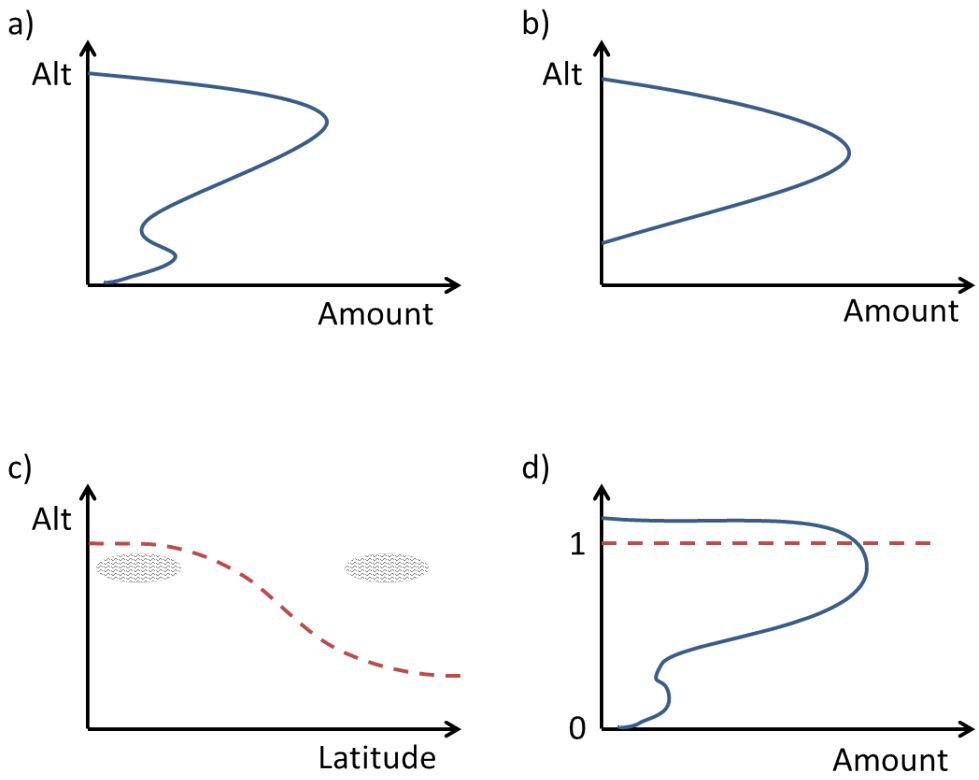


**Figure 3.2:** a) and b) show traditional ways of plotting the vertical extent of a plume, in terms of altitude and amount of $SO_2$, a) has heights retrieved at various altitudes and b) is a column generalised as a Gaussian. c) shows two plumes at the same altitude but different latitudes, leading to one above and one below the tropopause, and d) is the method which will be used here, in which the altitude of the plume is scaled around the height of the tropopause. In each case, the blue curves represent the plume profile, and the red lines, the tropopause height.

be found on either side of the tropopause. A way to get around this issue would be to scale the altitude axis with respect to the height of the tropopause itself. The total mass of $SO_2$ can still be calculated by the area under the curve, but by integrating above and below the tropopause level, it is also possible to estimate the mass of $SO_2$ in the troposphere and in the stratosphere, a representation of which can be seen in figure 3.2d.

The output for the Oxford IASI retrieval described in chapter 2, operates in terms of pressure levels, as established by RTTOV, but in this scenario it is more useful to work in terms of altitude: a linear scale throughout the atmosphere. This transformation requires some algebraic manipulation.

The relationship between the height of the tropopause and the height of the plume is derived from the barometric pressure equation:

$$P = P_0 e^{-\frac{z}{H}} \qquad P_T = P_0 e^{-\frac{z_T}{H}} \tag{3.1}$$

Where $P$ and $z$ are the plume altitude in terms of pressure and height respectively, $P_T$ and $z_T$ are the tropopause pressure and height respectively, $P_0$ is the atmospheric pressure at ground level, and $H$ is the scale height for troposphere[1], as defined by:

$$H = \frac{kT}{mg} \tag{3.2}$$

Where $m$ is the average mass of air[2], taken to be 28.8 $\text{gmol}^{-1}$. The relevant scale height here is calculated at the height of the tropopause. The height of the tropopause at any given location is derived from the barometric formula (equation 3.1). Through a simple combination of equations, and rearranging, the relationship between the height of the plume and the height of the tropopause can be derived:

$$z - z_T = -H(\ln P - \ln P_T) \tag{3.3}$$

The $SO_2$ profile is assumed to have a Gaussian profile shape as a function of pressure (as described in Carboni et al. (2012)), as described by:

$$\chi_{SO_2} = \frac{A}{\sigma_{SO_2}\sqrt{2\pi}} e^{-\frac{1}{2}\left(\frac{p - p_{max}}{\sigma_{SO_2}}\right)^2} \tag{3.4}$$

Where $\chi_{SO_2}$ is the volume mixing ratio of $SO_2$, here in units of parts per part, $p_{max}$ is the mean plume altitude, $\sigma_{SO_2}$ is the vertical spread of the plume, usually taken to be 100 mb, and $A$ is the total column amount of $SO_2$. The level of the tropopause is in actuality defined as the region of the atmosphere where the lapse rate changes from positive in the troposphere, negative in the stratosphere, or more accurately, where the rate of change of temperature with height tends to zero (defined as the region where the lapse rate is less that 2 $\text{Kkm}^{-1}$ by WMO (1957)). This is calculated for every IASI pixel from its associated ECMWF profiles, along

[1] The vertical distance over which the density and pressure fall by a factor of $1/e$

[2] `http://www.engineeringtoolbox.com/molecular-mass-air-d_679.html`

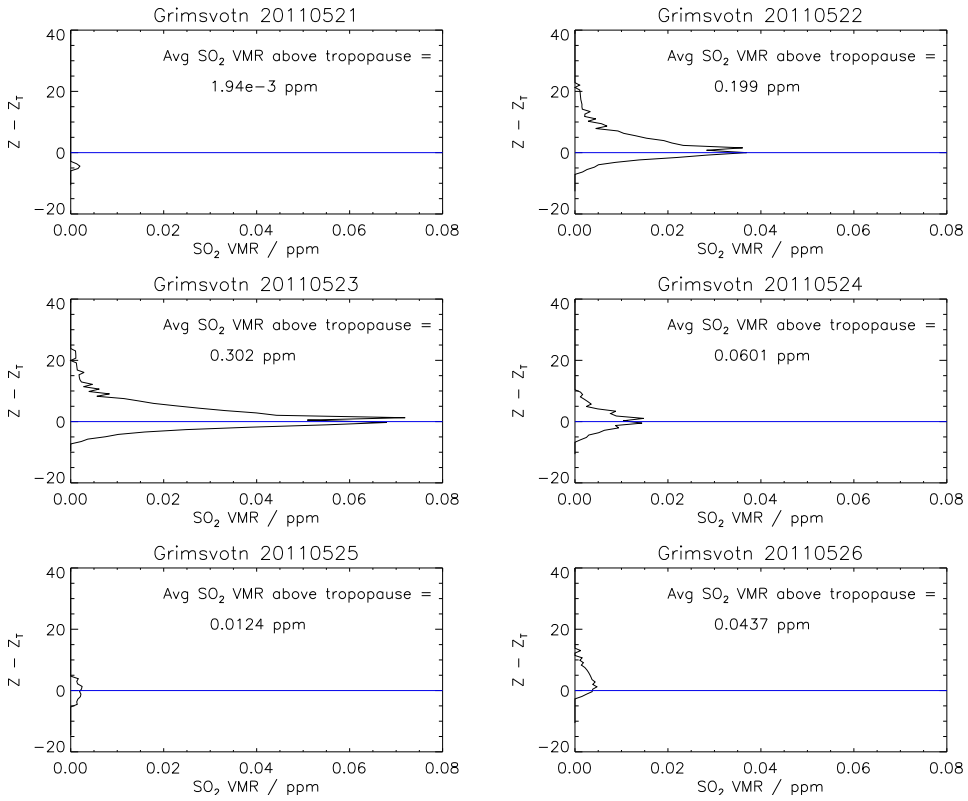


**Figure 3.3:** $SO_2$ loading from the individual days of the 2011 Grìmsvötn eruption. All plots are on the same scale, with the y axis representing the height in km above and below the level tropopause, and the x axis the concentration of $SO_2$ in ppm. The values for stratospheric $SO_2$ are an estimation of the total mass in ppm, as derived from the area under the distribution.

with the scale height for the same conditions. The pressure levels are regridded as defined by equation 3.3 and the $SO_2$ concentration is summed across the new altitude bins. The result of this can be seen for the 2011 eruption of Grìmsvötn in figure 3.3 and for the 2011 Nabro eruption in figure 3.4, along with a rough estimation of the mass of $SO_2$ in the stratosphere, which is calculated from the area under the curve.

The main differences which are made obvious in these plots are the altitude of the plume, and its longevity. The Grìmsvötn plots show an injection of $SO_2$ peaking at the level of the tropopause, though with more loading above. The main part of the plume then rapidly seems to dissipate over the following days, leaving behind an increased stratospheric loading. The Nabro plume, in contrast reaches a peak on the second day of the observations slightly below the level of the tropopause, although a significant amount was injected into the stratosphere and

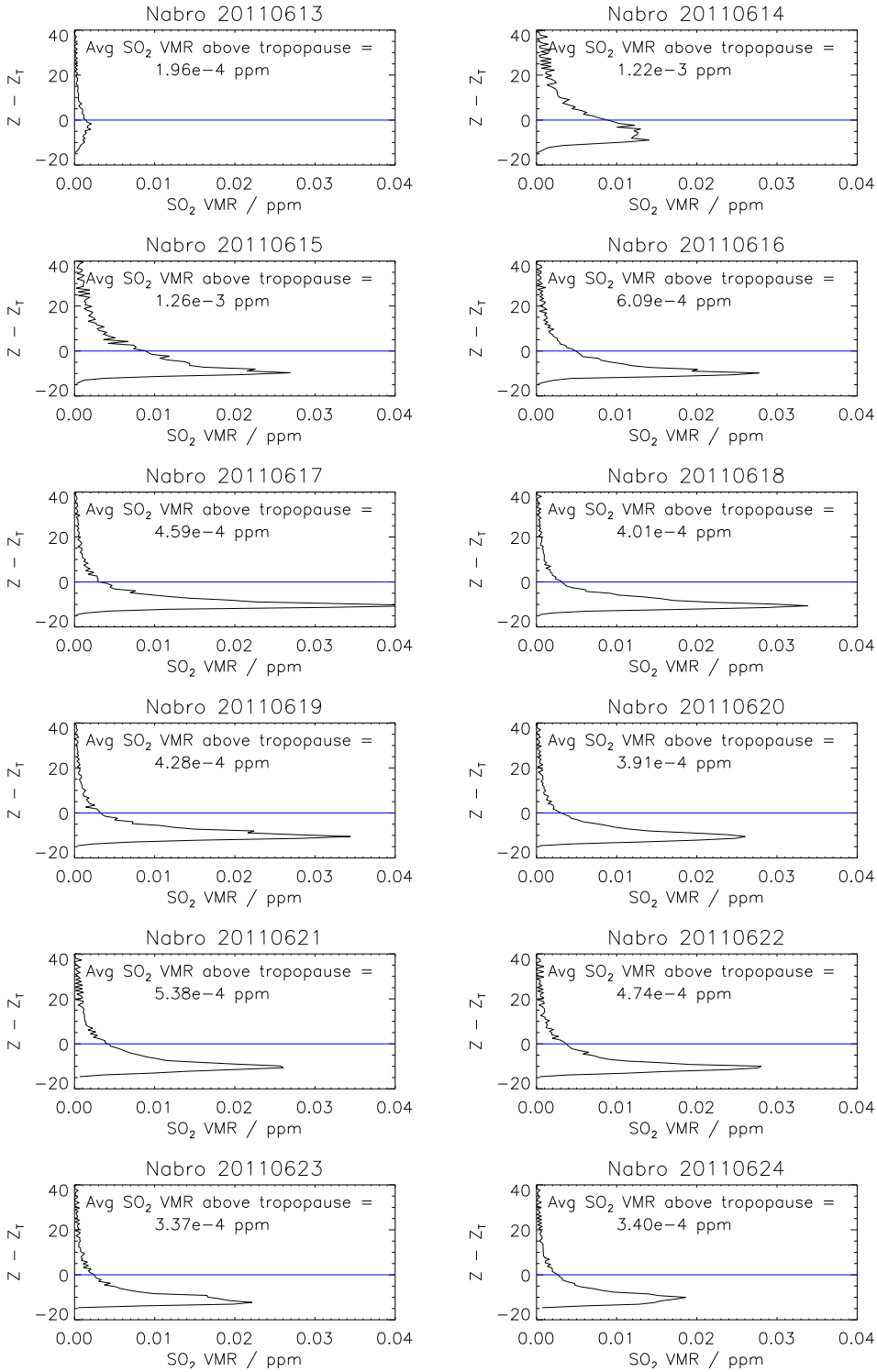


**Figure 3.4:** $SO_2$ loading from the individual days of the 2011 Nabro eruption. All plots are on the same scale, with the y axis representing the height in km above and below the level tropopause, and the x axis the concentration of $SO_2$ in ppm. The values for stratospheric $SO_2$ are an estimation of the total mass in ppm, as derived from the area under the distribution.

remains relatively consistent throughout the eruption. The large peaks lower in the troposphere are most likely due to a couple of reasons. The Toulouse Volcanic Ash Advisory Centre (VAAC) reported an almost continuous emission up until the 21st of June, the plumes rising to around 7 km and largely consisting of water and $SO_2$ (Venzke, 2013). This is very likely on the limit of what IASI can image, in terms of altitude, and could also very easily have been covered by higher altitude plumes, but would explain a contribution to the lower altitude peak than might be expected for such a large eruption. The main part of the plume was also observed to become entrained in the Asian Monsoon, where it was for the most part trapped for several days (Clarisse et al., 2014), which could also contribute to the apparently lower altitude peak in $SO_2$, and also the longevity of the peak. This height difference is of particular importance as there is still debate over the injection height of the Nabro eruption. Whereas it is clear that a significant amount of $SO_2$ has here been measured in the stratosphere, and as has previously been discussed is unlikely to have crossed the tropopause by atmospheric circulations alone, implying a stratospheric injection, the height of the peaks in this analysis and the known entrainment in the Asian Monsoon would also indicate an injection below the tropopause.

The oscillations at high altitude and low concentration are an artefact introduced by defining the plume as a Gaussian distribution. The tails either side of the peak, when combined with the gridding procedure, create these jumps. These could likely be removed by including a threshold concentration.

To calculate a more rigorous estimation of the $SO_2$ loading, each IASI profile is integrated following the equation shown in equation 3.4, to find the mass of $SO_2$ per unit of (surface) area. The result is then binned in latitude and longitude, averaged across the square bins and multiplied by the area of the bins (equation 3.6), taking account of the fact that, due to the curvature of the Earth, the bins are not quite square.

$$\text{kgm}^{-2} = \int_0^{p_t} \chi \frac{M_{SO_2}}{M_{air}} \frac{dp}{g} \tag{3.5}$$

$$\text{Area} = R^2 \Delta lat \Delta lon \cos(lat) \tag{3.6}$$

$M_{SO_2}$ is the molecular mass of $SO_2$, taken to be 64.0638 g $mol^{-1}$. Table 3.1 shows the results of these calculations as applied to all eruptions in the current Oxford IASI archive, as described in section 2.1.1, the eruptions of significant enough $SO_2$ loading to run the full IASI retrieval. Also presented here are the total volcanic contributions as averaged over the year for both the stratosphere and the troposphere, found by taking the loadings measured over the course of the individual eruptions, and averaging those over the whole year.

Figure 1.1 reports that an estimated 3500 - 5500 Gg S $yr^{-1}$ is added to the atmosphere through volcanism. It also reports an estimated total tropospheric and stratospheric loading, as contributed to by all known sources, of:

Estimated Tropospheric Loading $\simeq$ 400 Gg S = 0.4 Tg S

Estimated Stratospheric Loading $\simeq$ 12 Gg S = 0.012 Tg S

Through this work, values of 0.05405 Tg S for the tropospheric and 0.02557 Tg S for the stratospheric loading from volcanic sources have been derived (table 3.1). Although slightly skewed by potentially double counting the same $SO_2$ on subsequent days, the value for the stratosphere here derived is of the same order of magnitude as that derived by other groups. The value for the troposphere, on the other hand, is an order of magnitude lower than that estimated in figure 1.1. This is due to only eruptions likely to have resulted in a stratospheric injection of $SO_2$ being included in this analysis, and therefore missing out any and all smaller eruptions and degassing throughout the year. The estimations of $SO_2$ flux are many and varied, though the general opinion is that the contribution of passive volcanic degassing is between 2 - 14% of the total $SO_2$ flux from all sources (Bluth et al., 1993; Graf et al., 1997; Andres and Kasgnoc, 1998; Oppenheimer et al., 2011; Mather et al., 2013). This equates to between 2 - 28 Tg S $yr^{-1}$, so would easily cover the deficit left by the explosive eruptions. There are also many other sources of tropospheric $SO_2$ than volcanoes alone: biomass burning and anthropogenic sources, among others, will account for any deficits.

| | Stratosphere / Tg $SO_2$ | Troposphere / Tg $SO_2$ |
|---|---|---|
| **2008** | | |
| Llaima | - | 0.14 ± 0.14 |
| Okmok | 0.16 ± 0.07 | 0.13 ± 0.05 |
| Kasatochi | 1.49 ± 0.19 | 1.88 ± 0.25 |
| Dalaffilla | 0.17 ± 0.02 | 1.16 ± 0.15 |
| Yearly Average | 0.07 ± 0.08 Tg $SO_2$<br>0.04 ± 0.05 Tg S | 0.10 ± 0.11 Tg $SO_2$<br>0.05 ± 0.06 Tg S |
| **2009** | | |
| Sarychev | 1.01 ± 0.13 | 1.13 ± 0.15 |
| Yearly Average | 0.04 ± 0.005 Tg $SO_2$<br>0.02 ± 0.003 Tg S | 0.05 ± 0.01 Tg $SO_2$<br>0.02 ± 0.003 Tg S |
| **2010** | | |
| Soufrière Hills | 0.02 ± 0.02 | 0.06 ± 0.06 |
| Merapi | 0.20 ± 0.20 | 0.63 ± 0.63 |
| Nyamuragira | - | 0.49 ± 0.34 |
| Yearly Average | 0.01 ± 0.02 Tg $SO_2$<br>0.01 ± 0.02 Tg S | 0.03 ± 0.05 Tg $SO_2$<br>0.01 ± 0.02 Tg S |
| **2011** | | |
| Nyiragongo | 0.02 ± 0.01 | 0.86 ± 0.68 |
| Grìmsvötn | 0.44 ± 0.07 | 0.33 ± 0.05 |
| Puyehue | 0.08 ± 0.12 | 0.18 ± 0.28 |
| Nabro | 0.36 ± 0.15 | 6.68 ± 2.81 |
| Yearly Average | 0.03 ± 0.05 Tg $SO_2$<br>0.01 ± 0.02 Tg S | 0.28 ± 0.50 Tg $SO_2$<br>0.14 ± 0.25 Tg S |

**Table 3.1:** Calculated values for the total mass of $SO_2$ erupted from the given volcanoes over the course of the eruption, into the stratosphere and troposphere respectively, and the same values averaged over the year, with associated error terms

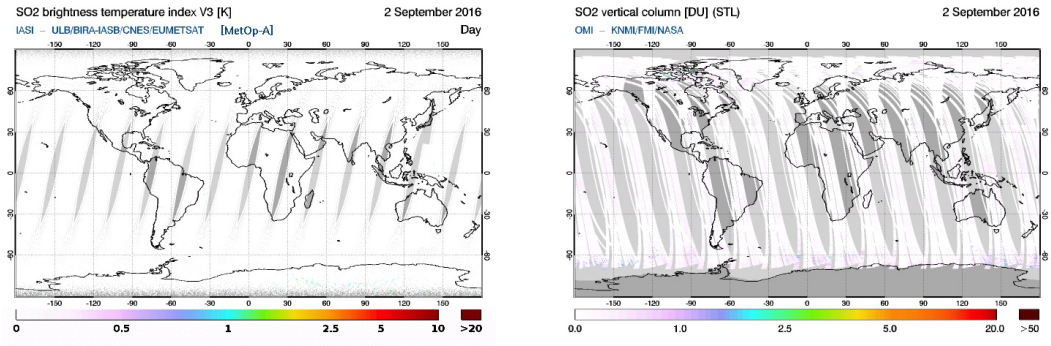


**(a)** IASI **(b)** OMI

**Figure 3.5:** A comparison of the area missed between satellite passes by the a) IASI, and b) OMI instruments, for the 2nd September 2016. Plots reproduced from the Support to Aviation Control (SACS) website[3]

The error in these calculated values is introduced by a number of sources, including the double counting already mentioned. When looking at 12 hours worth of IASI passes together (figure 3.5a), it is clear that a significant area is missed between successive passes between 30°N and 30°S. IASI has an advantage over instruments such as OMI (figure 3.5b) both in the space between tracks, and in the fact that IASI takes both a day and night scan, which largely covers the gaps left between them, averaging out over the two passes during the 24 hour period. The error associated with this missed data is therefore much greater over the equator than at the poles. Figure 3.6 shows a representation of how much of the Nabro plume was missed due to the gaps between passes for one 12 hour period, the error in which would be relatively high due to the missing data across the most concentrated area of the plume. From a manual investigation of days of the Nabro eruption, it can be estimated that as much as 25% of the plume is not detected by IASI: a significant error for equatorial measurements.The height of the plume may be assumed to be an interpolation of the heights on either side of the gap, but $SO_2$ concentration is clearly more complicated. An indication of $SO_2$ concentration, however, could be derived from other satellite measurements, such as OMI. In future iterations of this procedure, a scaling factor could be developed to account

[3]Royal Belgian Institute for Space Aeronomy, `http://sacs.aeronomie.be`, Near-Real-Time archives.

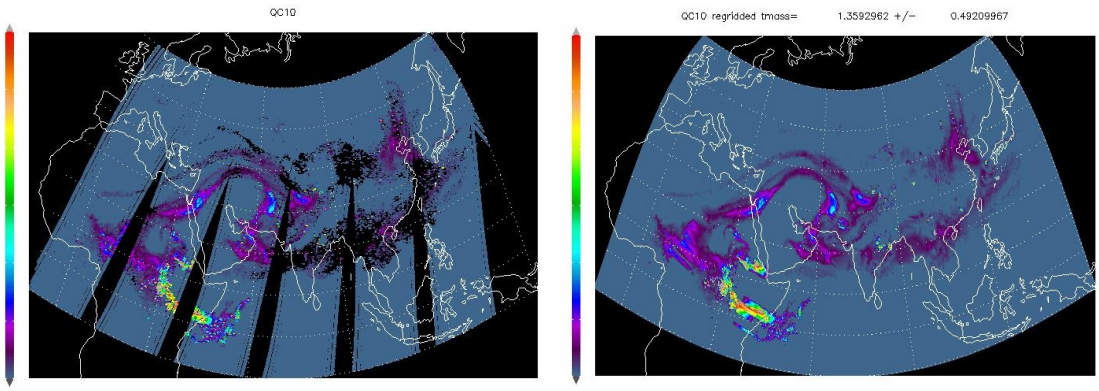


**Figure 3.6:** Retrieved $SO_2$ field from IASI, from the pm pass on the 18th of June: $SO_2$ can be seen to be emitted in Eritrea, move north and east, and become entrained in the Asian monsoon. Left, the direct result of combining tracks, and right, with the interpolation over the gaps.

for this latitude dependent error term. The uncertainty here can be quantified by comparing pixels either side of a gap between two tracks. In the case of a plume of equal $SO_2$ concentration either side of the gap, the plume can be interpolated across. If, however, a plume covering the edge of one pass but with no plume present in the adjacent pass, interpolating across the gap will result in a larger plume than expected and therefore a larger uncertainty term (see figure 3.6).

Another large error term is provided by the retrieval output itself, which is a combination of the error in the instrument and in the retrieval. The analysis procedure includes a step to filter for the larger errors, but those remaining are still on the order of ± 10 - 15% for Nabro, and ± 6 - 10% for Grìmsvötn, for example. Any large error terms in table 3.1, on the order of 100 % of the calculated values, are likely due to either the IASI tracks leaving a gap across the main body of the plume, or the plume having a high ash content.

The other measurement with an associated error is that of the tropopause height. If the height of the tropopause is changed by 1 km, the total stratospheric mass changed by between 5 and 15% and the tropospheric between 0.03 and 9%, averaging to 7.5 and 4.8 % respectively, in practice, however, this term is largely drowned out by the other larger error terms.

To increase the accuracy of these estimations, an issue to overcome would be the potential for counting the same $SO_2$ plume on subsequent days. Though reduced by

the averaging procedure, in order to remove this completely the individual plumes would have to be tracked from image to image, with only any new emissions added to the sum. This is theoretically possible with the application of a trajectory model to track the movements of air parcels, but would also rely on what can manually be observed, either in the outputs from the IASI retrievals themselves, or from an instrument such as MODIS with cameras but relying on an lack of cloud cover. Both of these methods also have inherent problems, be that in tracking wind speeds over a long period of time, or in trusting to human selection of separate plumes, but have the potential to give a more accurate estimate.

### 3.1.1 Scale and Latitude

The eruptions investigated in table 3.1 can also be plotted in terms of latitude for the individual years. This can provide clearer insight into the relative scale of the eruptions, and the extent in latitude.

The $SO_2$ emissions from these eruptions were regridded to show only the vertical and latitude planes, ignoring any longitudinal extent. The atmospheric loading for each eruption was averaged over the course of the year. The results from 2008-2011 can be seen in figure 3.7.

There appears a general trend in these plots towards bigger eruptions occurring in the northern hemisphere, in particular around 50°N, though the majority of volcanoes are situated in the mid latitudes. The apparent smearing upwards on the plot is an artefact resulting from plotting in terms of pressure levels (which get further apart at higher altitudes). This shape would disappear therefore, if figure 3.7 were plotted in terms of altitude, but this would mean altering the retrieval.

With this form of analysis, the relative sizes of eruptions becoming apparent. When plotted individually, the eruption of Puyehue in 2011 appears far larger that any other eruption, with $SO_2$ clearly discernible for a month after the initial eruption, and spread over much of the southern hemisphere (see Carboni et al. (2016)). However, when compared with the much greater quantity of $SO_2$ emitted

**(a)** 2008 - Llaima, Dalaffilla, Kasatochi, Okmok

**(b)** 2009 - Sarychev

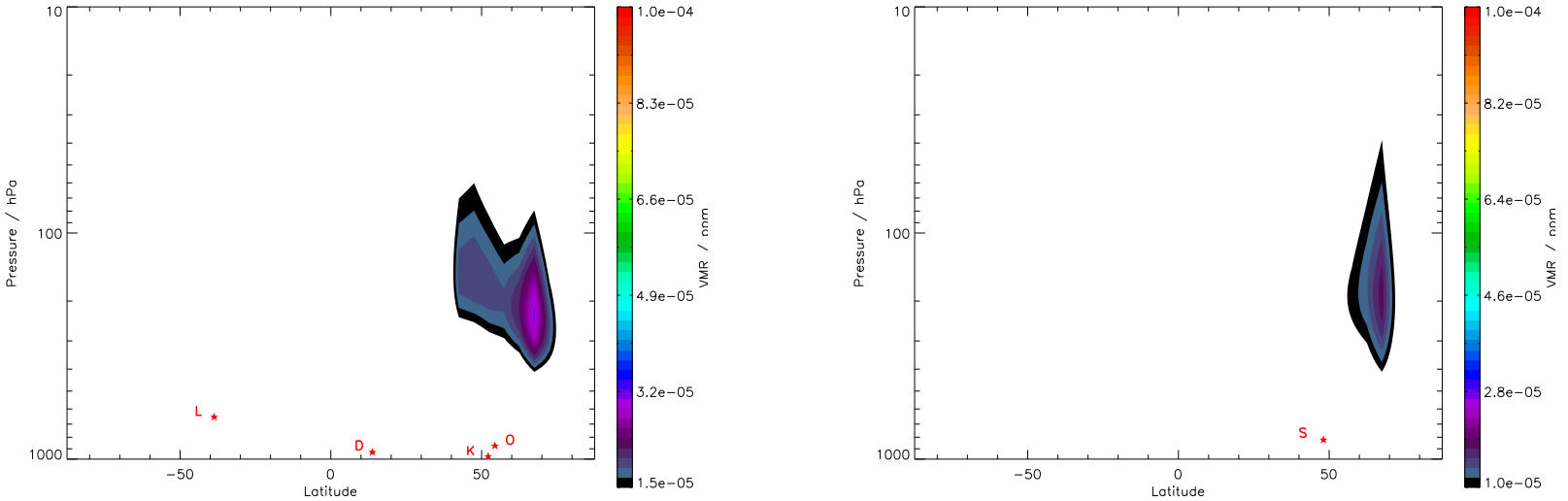


**(c)** 2010 - Merapi, Nyamuragira, Soufrière Hills

**(d)** 2011 - Puyehue, Nyiragongo, Nabro, Grìmsvötn

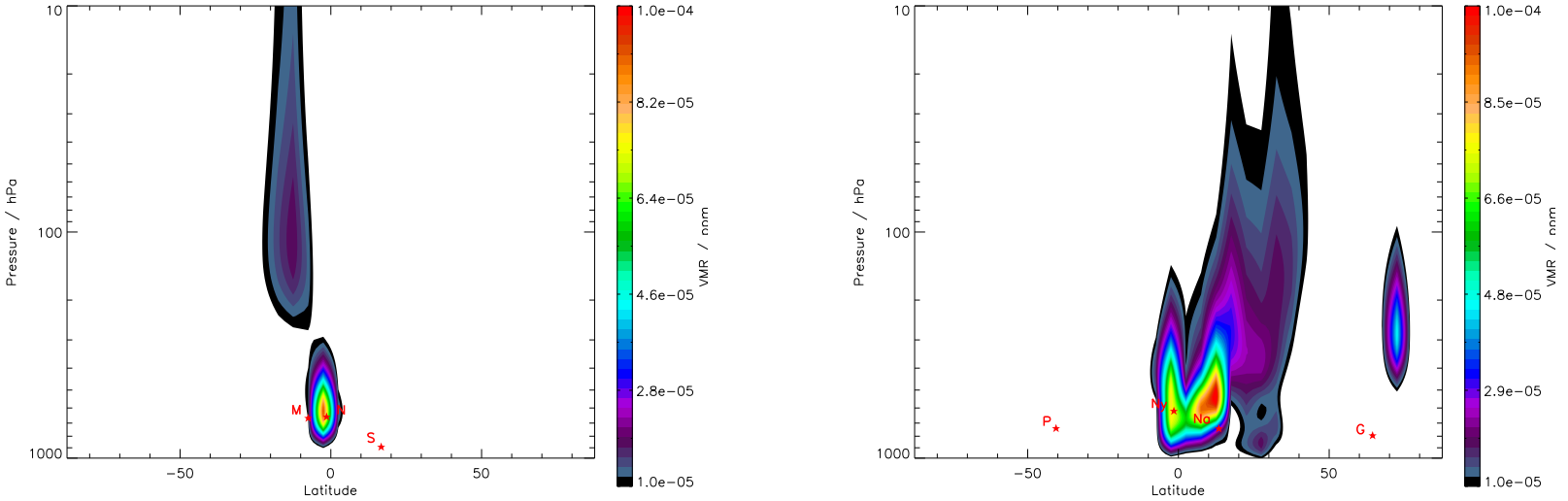


**Figure 3.7:** Global $SO_2$ loading retrieved by IASI, and averaged over the year to give a daily average $SO_2$ volume mixing ratio (colour table). The red stars represent the latitude and altitude of the relevant volcanoes

by Nabro, for example, and over a shorter time frame, the relatively low magnitude of the eruption becomes clear.

## 3.2 Conclusions

From the investigation normalising about the level of the tropopause, the value for the stratospheric loading presented is of the same order of magnitude as those found in literature, with that of the troposphere an order of magnitude lower. Although partially explainable due to the methodology, for example only using the emissions from explosive eruptions, there are also significant error bars on these values, in general around 12% error for the troposphere and 20% for the stratosphere, but reaching as high as 50-60% for some days over equatorial regions. Some errors are inherent in the system, such as the area missed between the IASI passes, the major problem to overcome is counting the same parcel of $SO_2$ on multiple days. Although mitigated through averaging, this still presents a significant but largely poorly understood error term.

# 4
# HYSPLIT Trajectory Studies

The aim of this chapter is to produce, and establish the suitability of, a forward model for the trajectory of a sulphur dioxide plume, and to perform a proof of concept using two well observed case studies. A series of trajectories will be calculated at various starting altitudes and times using NOAA's HYSPLIT trajectory model, and the end points of these paths will be compared against IASI volcanic data. It is also hoped that this approach will reveal some information about the evolution of the $SO_2$ amount, as it is converted into $H_2SO_4$ aerosol, and the change in plume altitude over time.

## 4.1 Background/Introduction

The aim of this section is to use modelled trajectories to predict the movement of volcanic plumes. The success of this method is investigated by comparison with IASI retrievals of $SO_2$. If the process were to prove valid, this could be extended to forecast meteorology, and be used as a method of hazard prediction, as so many of the historical studies have been: if the position of the plume could be accurately calculated a day or so after the initial injection, then this could be extended with forecast meteorology to predict any human impact, such as aviation, and covering areas of significant population. Single images of a plume show the

spacial evolution of the plume, but do not give any incite into the changes within the air parcels: it is hoped that this approach will.

The model chosen for this study was the Hybrid Single Particle Lagrangian Integrated Trajectory Model, or HYSPLIT, as developed by the Air Resources Laboratory at the National Oceanic and Atmospheric Administration (NOAA).

HYSPLIT was first developed in the early 1980s, as detailed in Draxler and Taylor (1982). The model went through many iterations until the late 90s, until version 4, which is the most recent model for trajectory analysis Draxler and Hess (1998). Since then there have been attempts to incorporate chemical transport and decay terms, as well as wet and dry deposition, but these play no part in the basic trajectory calculations (Stein et al., 2015).

A Lagrangian model for air pollutant concentrations, such as HYSPLIT, is one in which the parcel/particle advection and the diffusion terms are calculated independently and individual air parcels are tracked as they move through time and space; in contrast with the Eulerian method which focuses on points fixed in space through which the air flows. Lagrangian methods are well suited to scenarios with a single point source, and as such are ideal for studying volcanic eruptions. The HYSPLIT model is, in general, something of a mix of the two methods, but the advection and diffusion calculations are performed in the Lagrangian framework whereas it is the concentrations which are calculated on a fixed grid Draxler and Hess (1998). The horizontal and vertical wind terms can be defined by most meteorological datasets (Stein et al., 2015), and are interpolated onto the chosen model grid to compute the required trajectories. The main improvement of HYSPLIT_4 over previous iterations is that the interpolation of the meteorology in time, to the points required by the by the user, is performed as part of the trajectory calculation itself, giving much more flexibility.

The following section explores the history of trajectory analysis, primarily from volcanic sources. This is by no means meant to be an exhaustive investigation, but merely to give an overview of the techniques used.

### 4.1.1 Volcanic Trajectory studies

There have been a number of previous attempts to model the movement of volcanic plumes, the primary reason for which is the hazard aviation, other industries and to human habitation.

The early to mid 1990s saw a surge in studies of volcanic plume trajectories, presumably due to the two large eruptions in 1991 of Pinatubo in June, categorised as the biggest of the 20th century (Ramachandran et al., 2000), and Cerro Hudson in August, which although smaller, its latitude resulted in a long lived plume (Schoeberl et al., 1993). The vast majority of these trajectory studies focus on ash, due to its greater risk to the aviation industry compared with $SO_2$ (Prata et al., 1991).

Schoeberl et al. (1993) sought to understand the evolution of the $SO_2$ plume from the Cerro Hudson eruption, and matched their modelled plume trajectories to the observations of the Total Ozone Mapping Spectrometer (TOMS). A lack of wind shear in the region of the initial injection meant that their model was relatively accurate up to 7 days after the eruption. In the model, the gas parcels were advected by winds which were interpolated in time and space onto the parcel positions from a 2 degrees latitude by 5 degrees longitude global grid and winds were calculated from a balanced flow approximation[1]. From their analysis, Schoeberl et al. (1993) find that the polar stratospheric region is very nearly completely isolated from that of the mid-latitudes, at least during late August, as they find little or no transport of $SO_2$ between the regions. They do not, however, seek to understand the evolution of the composition of the plume.

Searcy et al. (1998) also developed a preexisting model, which they refer to as PUFF, for use as a hazard warning of young ash clouds when satellite data was unavailable, due to cloud cover for example, and as such is designed to operate quickly. The original model was first developed in 1991 by Tanaka (1994), but was limited to volcanoes in the Cook inlet region of Alaska. Searcy et al. (1998) based their calculations on Tanaka's three dimensional Lagrangian formulae for

[1] A set of equations describing the behaviour of one isolated parcel of air of constant density moving on a horizontal plane. The pressure, friction and Coriolis forces acting on the parcel are in balance

pollutant dispersion. PUFF initialises a subset of ash particles, representing a sample of the eruption cloud, and calculates transport, turbulent dispersion, and fallout for each particle individually. The advection is calculated for each particle by interpolating four-dimensional wind data to the particle's position and time and moving the particle for a defined unit of time, similarly to Schoeberl et al. (1993) above. The four dimensional wind fields are derived from forecast meteorological data generated by the National Meteorological Center (NMC), a 2.5 by 5 degree latitude/longitude grid, with 10 vertical levels. What set PUFF apart for its time was the inclusion of the fallout rates, clearly vital for hazard awareness applications. Case studies were reported when AVHRR data was available for comparison. As was required by the application, Searcy et al. (1998) report that the model was indeed able to be run on the order of minutes, and was found to give a good estimate for the plume location on the order of days after the eruption, the accuracy of such results dependent on that of the forecast meteorology, and quantitative results not necessarily being required. They did, however, find that their plumes were often much larger than those observed by AVHRR, indicating that a significant loss term must be missing from their algorithm.

Bursik et al. (2009) developed upon a previous ash model, the Active Tracer High-resolution Atmospheric Model ATHAM, with the aim of estimating ash eruption rates. ATHAM is a plume model first developed by Oberhuber et al. (1998) to simulate explosive eruptions under standard atmospheric conditions. Bursik et al. (2009) took the standard atmosphere described in the original ATHAM model, combined with a "plume-centred coordinate system (BENT)", to develop an integral model of plume motion from an explosive eruption, within a variety of wind conditions. They state that trajectory analysis in general is difficult for ash plumes due to the variation in grain size, although they manage to model the plume movement of their chosen case studies, and the fallout from prehistoric eruptions, relatively well by using a wind field which varies with height. Due to the locations of the case studies used, they also had problems when the plume encountered the jetstream: eruptions with highly variable mass eruption rates were

preferentially entrained in the jetstream. They close by warning aircraft against using the jetstream to reduce journey times at times following a recent eruption.

Kristiansen et al. (2010) take a different approach to their plume trajectory studies. Using the 2008 Kasatochi eruption as a case study, they simulate the $SO_2$ vertical emission profile which is then perturbed by winds. The total column amount of $SO_2$ was determined from satellite observations from GOME-2, OMI and AIRS during the initial 48 hours after an eruption, and FLEXPART (Stohl et al., 1998), an atmospheric transport model, was applied to derive the vertical distribution and dispersion. In this model, trajectories of small air parcels are calculated as they are displaced by the winds, with meteorological data provided by ECMWF: 91 vertical levels with a resolution of 1 by 1 degrees horizontal resolution. A set of higher resolution (0.5 by 0.5 degrees) meteorological datasets was used for the area around the volcano (180–120° W, 40–60° N). $SO_2$ loss by reaction with the OH radical and dry deposition were also considered in the analysis: monthly averaged three-dimensional OH concentrations from the GEOS-CHEM model (Bey et al., 2001), were used to estimate the mass loss by reaction with OH. Overall, they found good agreement with the plume position determined by the three satellites used, and with ground based measurements. The model did, however, struggle with the 3 separate injections during the Kasatochi eruption, and so it was assumed that all the $SO_2$ was injected together.

A more recently developed ash focused transport model is the PlumeRise model, developed at the University of Bristol (Woodhouse et al., 2013). The main purpose of the model is to estimate plume heights from the source mass flux, but it can also be inverted to infer the flux from the plume height. The model was run under a number of different scenarios, such as a strong and weak eruptions, with and without wind shear (Woodhouse et al., 2016). They confirmed that these two parameters have far more effect on each other than any change in atmospheric conditions, such as wind speed or relative humidity. In this presented study, only theoretical eruptions have been used and no comparison was made to historical eruptions.

Although not used for studying volcanic plumes, McQueen and Draxler (1994) used back trajectory analysis to study plumes from oil fires, specifically those in Kuwait in 1991. They used satellite observations of the plumes from AVHRR to determine the plume centres and generated back trajectories from those points by using the National Weather Service Medium Range Forecast global model. The back trajectory would provide an estimate for the altitude of the plume. It was found that the error in the final positions of the trajectories was around 10% of the total distance travelled when using a fine meteorological grid, but rose to 14% when using a coarse grid, highlighting the importance of choosing a fine enough model resolution, but the fine grid was also far more sensitive to changes in the trajectory starting height.

### 4.1.2 HYSPLIT studies

In past studies, HYSPLIT has been used primarily to confirm plume altitudes, as the wind shear is assumed to be significantly different across the range of expected altitudes. This is especially useful when there are multiple plumes, as in the case of Prata and Kerkmann (2007), who used HYSPLIT to validate, and estimate the height of, two $SO_2$ plumes and one ash from the 2005 eruption of Karthala volcano in the Comoros Islands, Boichu et al. (2015) who confirmed the altitudes of multiple plumes from Etna, or Carn et al. (2015) studying $SO_2$ retrievals for the February 2013 eruption of Paluweh, Indonesia, from OMPS. An example of the results of such an application of HYSPLIT can be seen in figure 4.1. An additional application would be to determine an estimation of the plume age, as used by Schumann et al. (2011) for the Eyjafjallajökull ash plume.

HYSPLIT is a useful tool simply to validate an observed plume position, or a plume which is perhaps has a low concentration of $SO_2$ and therefore a high error in the retrieval, such as in the case of Carn et al. (2007), who used OMI to observed a long lived plume from Soufrière Hills in 2003, but which was elongated across the Atlantic Ocean.

HYSPLIT can also be set up as a dispersion model, as used by Adame et al. (2015) so study the transport of volcanic ash to Spain. The model is set up in

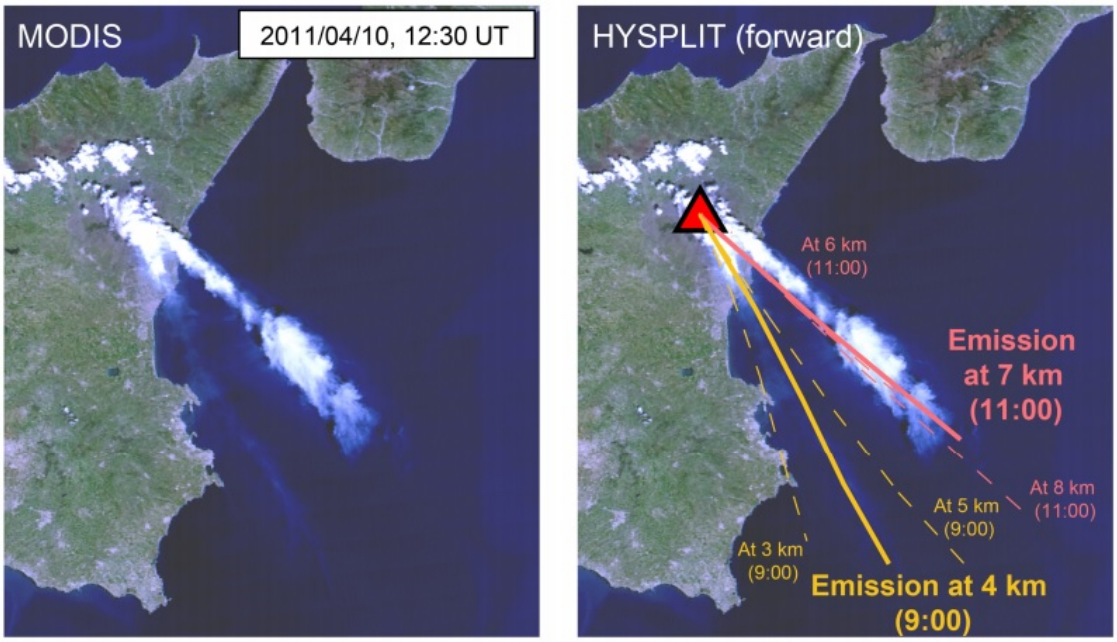


**Figure 4.1:** Image and caption reproduced from Boichu et al. (2015) MODIS/AQUA RGB image of Etna plumes on 10 April 2011 at 12:30 UT obtained from visible channels. (Right) Same as left panel, overlaid with the forward trajectories from the HYSPLIT model initialized with (yellow line) an emission at 4 ± 1 km a.s.l. starting at 09:00 UT and (pink line) an emission at 7 ± 1 km a.s.l. starting at 11:00 UT

much the same way as the trajectory analysis, with input parameters such as meteorological fields and the location of the source. The atmospheric wind at the top of the plume controls the dispersion of the volcanic material, but the emission height profile is difficult to determine from satellites alone. In this case, a uniform vertical distribution from the volcano summit to the top of the ash column has been used. It was determined that the estimated probabilities of an ash plume travelling over Spain are elevated for those volcanoes located to the west of Spain, due to the general atmospheric circulation.

## 4.2 Algorithm

The algorithm for finding the position of $SO_2$ at a given time after an eruption involves both HYSPLIT_4 model trajectories and IASI retrieved data. An overview of the procedure is displayed in figure 4.2.

Before any analysis can take place, the trajectories are generated using the online

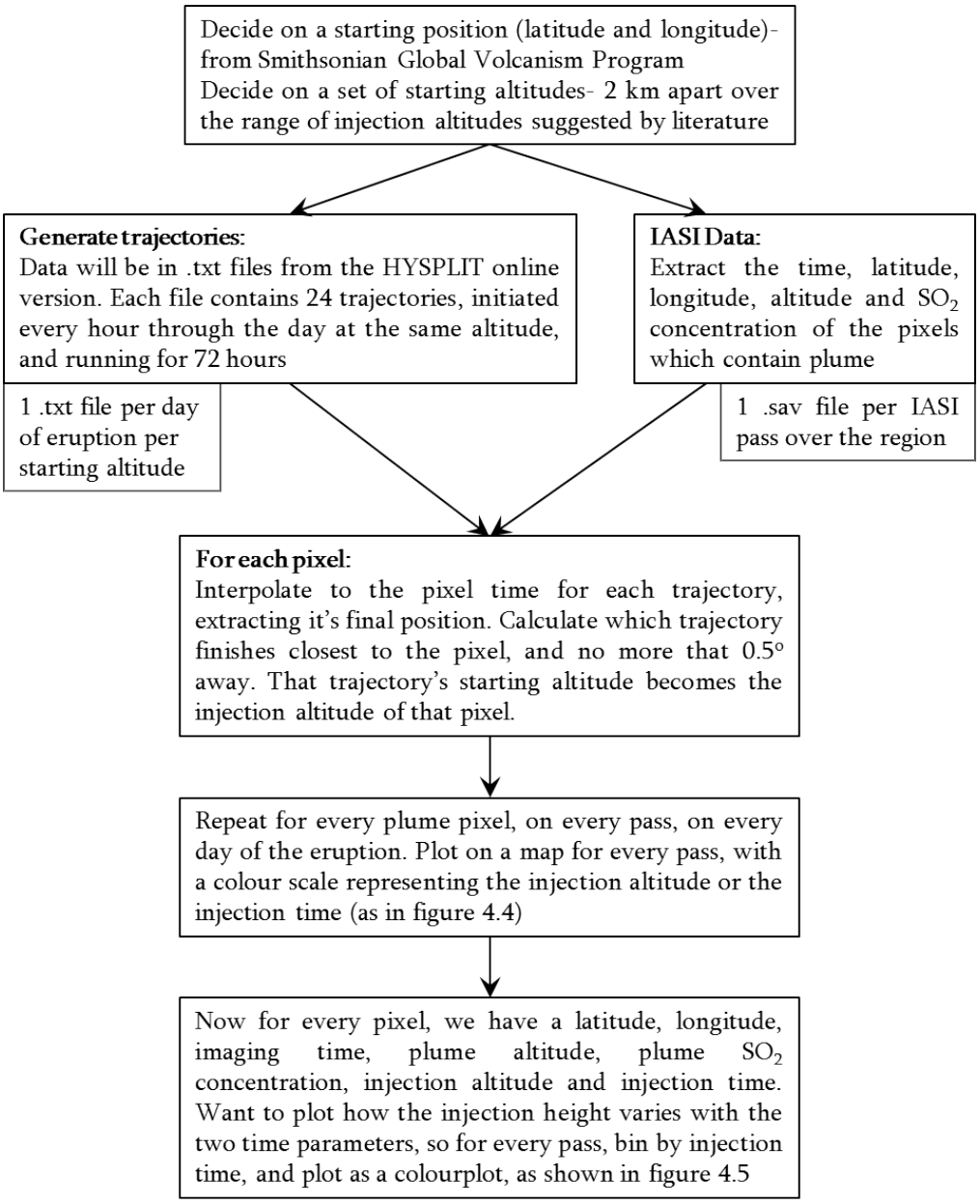


**Figure 4.2:** A visualisation of the algorithm developed here, for combining HYSPLIT modelled trajectories with IASI retrieved $SO_2$ fields

version of the HYbrid Single-Particle Lagrangian Integrated Trajectory (HYSPLIT) model. The starting time, starting position in latitude and longitude, starting altitude and the frequency and duration of the trajectories are all set independently at this point. The meteorological model GDAS0p5 was chosen for this study for its high horizontal resolution of half a degree latitude/longitude. GDAS0p5[2] is a global 3-dimensional gridded meteorological model, containing output data at 3-hourly intervals and at half degree/half degree horizontal resolution. The vertical resolution of the trajectory analysis is clearly dependant on the vertical resolution of the particular meteorological data used. The dataset used in this study used hybrid sigma-pressure levels, with the closest spacing of vertical levels in the low to mid troposphere. Averaged over the the entire vertical extent of the model, 0 - 18 km, the average spacing of vertical levels works out at approximately a new level every 327 m. NOAA ARL, where HYSPLIT is run, processes the model output and interpolate it onto the same grid on which HYSPLIT operates.

The duration of the trajectory generated was always set to 72 hours. This is the maximum duration of the available version of HYSPLIT and long enough to establish the overall direction of plume travel. Any longer than 72 hours and NOAA estimate a large amount of uncertainty in the final positions: NOAA quotes between 200 and 700km after 96 hours (Rolph and Draxler, 1990). HYSPLIT only generates a new trajectory every three hours, meaning that this is technically the minimum temporal resolution. Any temporal grid finer than this will have been interpolated by the model, but barring any extraordinary weather conditions, smaller time steps down to an hour did not give any dramatically different results. Time intervals of 6 hours between trajectories were found to miss significant changes when interpolated.

The starting position of the trajectories in latitude and longitude is simply the location of the volcano, and was taken from the Smithsonian Global Volcanism Program database (Venzke, 2013). A grid of starting altitudes was established in each case from previous studies, a number of kilometres either side of the generally agreed injection altitude. In all cases reported here, altitude steps of 2 km were

[2]Global Data Assimilation System (GDAS) model (`http://www.emc.ncep.noaa.gov/index.php?branch=GFS`)

used. Steps of 1 km and 500 m were also tested, but found that interpolation to the same levels from 2 km steps made minimal difference in the output for the days tested: variation on the order of 250 m in injection height, between the 500 m trajectories and the 2 km trajectories interpolated down to every 500 m, but with an increase in time, both to generate the trajectories and to run the analysis, of many hours. Taking a point directly above the volcano is assuming a directly vertical injection, with no wind shear, and the volcano is treated as a point source, with the initial horizontal extent of the plume considered negligible when compared with the overall plume movement. These trajectories are known as "forward" trajectories, as opposed to "backward" trajectories which are initiated at the plume and traced back to a probable source. In this study forward trajectories are more appropriate: attempting to generate back trajectories would mean either generating one for every pixel of every scene, which would be massively computationally expensive and time consuming, or generalising to a mathematical plume centre, and therefore losing information about the chemical evolution; forward trajectories are also imperative if the method is ever going to be applicable to predictive applications. It is far more useful, therefore, to generate trajectories at a number of initial heights and follow them forwards, selecting the ones which follow the course of the plume. The starting time of the trajectories are also derived from the literature. Given the maximum trajectory duration of 72 hours, the first trajectory is started three days before the first time the plume was observed. This is to take into account any portion of the observed plume which was erupted before the main eruption, or which is part of any degassing. Otherwise, the trajectories are generated for all days on which a plume was observed.

It is at this point that the IASI data is first brought in. From the $SO_2$ retrieval, the time and position data of each pixel observed as containing $SO_2$ are used to establish the time at which the end of the trajectories must be read off. The data is treated orbit by orbit. For each IASI data file, the data is read in, the time of each pixel is extracted and used to cut off all trajectories which pass through that time. If that time falls between two calculated points, those points are interpolated to

the correct time. This is done for every set of trajectories at each starting altitude (injection altitude). Once the positions are calculated, they are then compared back to the IASI image, and for each point, the trajectory which passes closest to that point at the time the IASI data was taken is extracted. The distance of the trajectory from the IASI pixel is calculated using spherical polar coordinates as shown in figure 4.3 and equations 4.1 and 4.2.

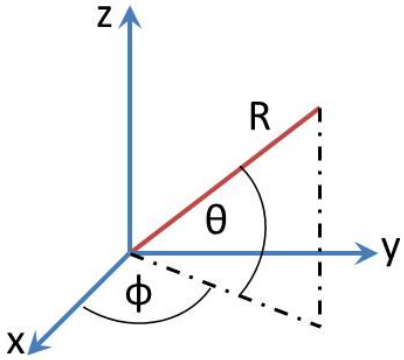


**Figure 4.3:** Cartesian vs. Spherical polar coordinates

$$\begin{aligned} \theta &: \text{ latitude } \; -90 \leq \theta \leq 90 \\ \phi &: \text{ longitude } \; 0 \leq \phi \leq 360 \end{aligned} \tag{4.1}$$

$$d^2 = 2 - 2\cos\theta_1 \cos\theta_2 \cos(\phi_1 - \phi_2) - 2\sin\theta_1 \sin\theta_2 \tag{4.2}$$

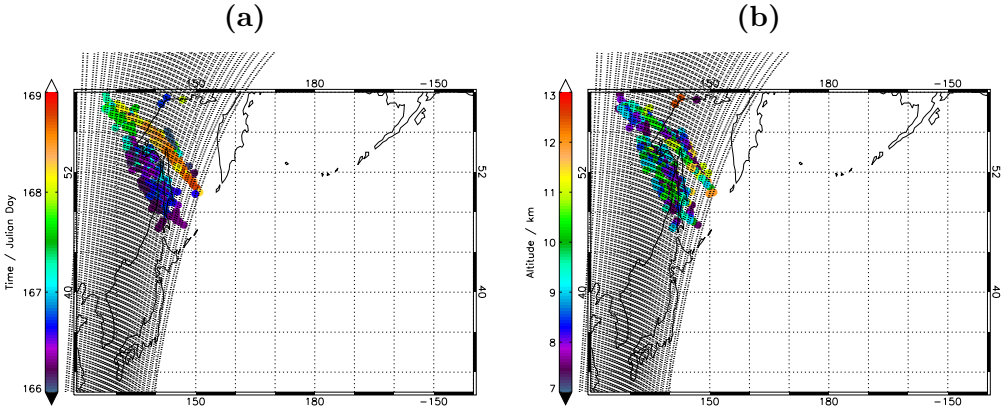


**Figure 4.4:** The IASI pass over the Sarychev region, starting at 0105 UTC. The colour bars represent a) the injection time and b) the injection height, as retrieved by the HYSPLIT trajectory analysis and the small black dots are the IASI pixels, plotted here to represent the path taken

The result when plotted over a map will be similar to that shown in figure 4.4, with a colour scaled distribution, here shown with the IASI path plotted in black. The map of the injection time (figure 4.4a) clearly shows the most recently erupted $SO_2$ closest to the volcano with the oldest further away, and the path taken by the plume is fairly clear. Each point at the end of a trajectory will have not only an initial injection altitude associated with it, but also a plume altitude and $SO_2$ concentration from the original IASI data. The simulated injection time can now be plotted against the median time of the IASI measurements, with either the injection altitude or $SO_2$ concentration at the end of the trajectory as a colour scale. The horizontal bars represent individual IASI orbits: originally, IASI orbits were averaged over a 12 hour period, so as to represent the ascending and descending IASI passes, but this was found to occasionally wildly skew the distributions when the $SO_2$ experienced an apparent rapid drop in altitude. Vertical columns represent a single parcel of gas injected at the time indicated by the horizontal axis. Using this method of plotting, it is possible to assess any trends in the results. For example, it should be possible to see a decay in the concentration of $SO_2$ in one particular air parcel as time increases, which would be seen as a difference in colour down the vertical columns, an idealised version of which can be seen in figure 4.5a.

The altitude of the plume at the time of the measurement can also be plotted. The retrieval outputs a height in terms of pressure, which can then be converted into the associated altitude. It is worth noting, however, that the conversion is not a simple one. The height associated with an atmospheric pressure is dependant on a number of factors, including the lapse rate (as described in chapter 3.1 when discussing locating the height of the tropopause). A detailed derivation of the process is described in Appendix A. In an ideal plot of the injection altitude, such as that shown in figure 4.5b, it would be expected that all subsequent measurements of the same parcel of gas would return the same injection altitude as the initial measurement, and therefore the columns in the colourplots would be all the same colour.

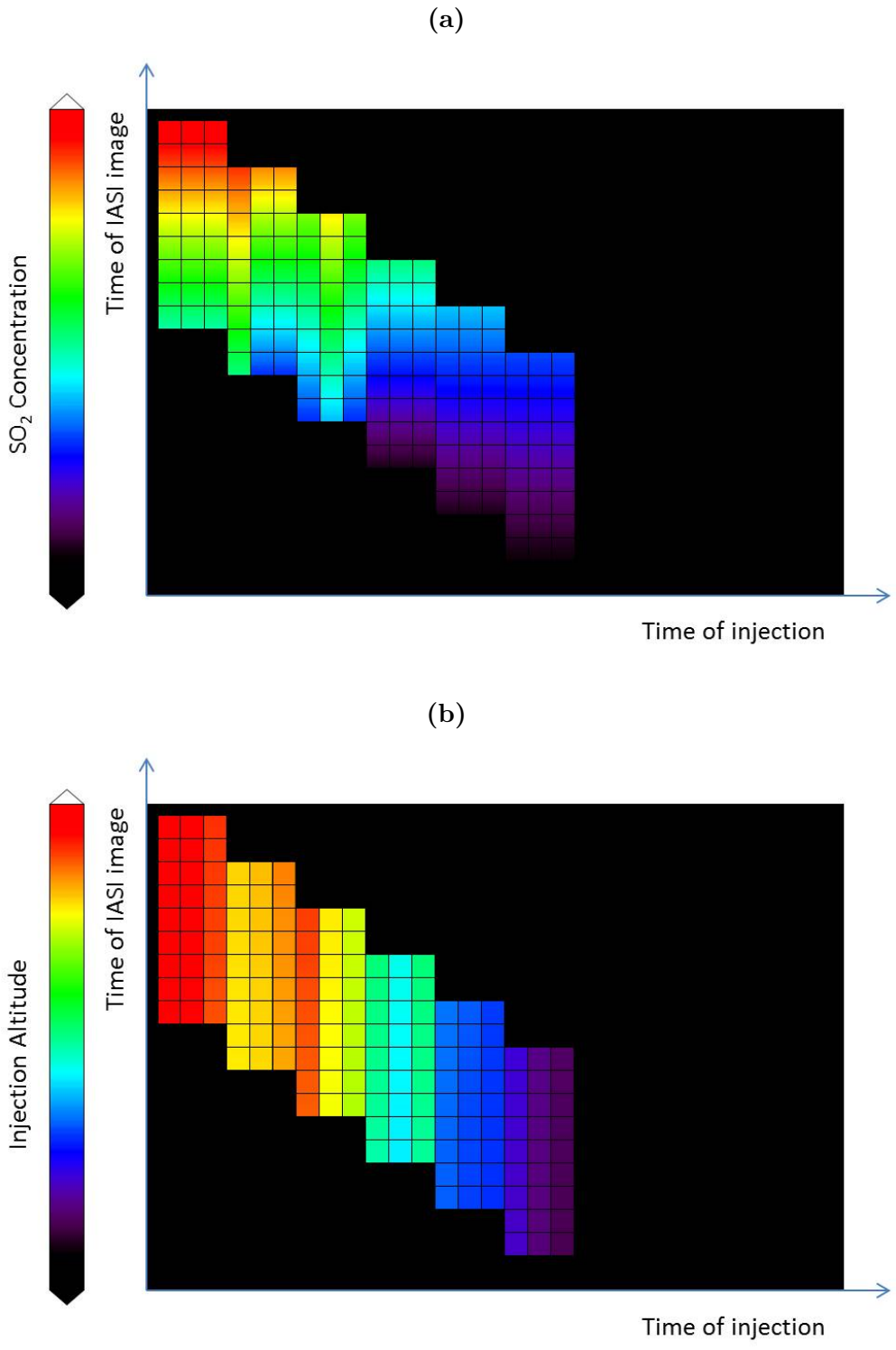


**Figure 4.5:** An idealised representation of a) the $SO_2$ concentration colourplots, and b) the injection height colourplots. In both cases, the vertical columns represent a single parcel of air, injected at the time indicated by the horizontal axis, and observed at various times as indicted by the vertical. The red end of the colourbars represent higher concentrations/altitudes.

The trends along the horizontal axis will depend on the nature of the individual eruptions. The case described in figure 4.5 shows an initial high altitude injection of high $SO_2$ concentration, and further lower altitude continuous injection over the duration of the study.

A representative error in the plume injection height was also calculated. Assuming that each vertical column shown on the injection altitude colour bar plots (for example, figure 4.7) represents one parcel of $SO_2$, then a mean calculated altitude can be taken of these values, the standard deviation of which is the associated error. The two case studies presented here largely escape the problem of gaps between the IASI passes presented in the previous chapter, however in the case of lower latitude eruptions this may again cause errors in attempting to track individual air parcels over the course of several days.

## 4.3 Case study Kasatochi

Kasatochi is a stratovolcano[3] located in the central Aleutian Islands of far western Alaska. As Waythomas et al. (2010) reports: it "erupted violently on August 7, 2008 after an intense period of precursory seismic activity. Kasatochi has received little study by volcanologists and has no confirmed historical eruptions." The island was a long term research site for the US Fish and Wildlife Service (USFWS). On the 4th of August, they contacted the Alaska Volcano Observatory (AVO) after feeling small tremors. Small earthquakes, and even larger ones, are relatively common for the area, but by the 6th of August significant volcanic activity became apparent. On the morning of the 7th, a magnitude 5.8 earthquake occurred within a few kilometres of the island. Soon after, seismic instruments on the nearby Great Sitkin Volcano recorded strong tremors consistent with movement of fluid, either gas, magma or both, which is often seen just before an eruption. That afternoon, satellite images confirmed that Kasatochi was indeed erupting.

The afternoon of the 7th of August saw three distinct eruption events: at approximately 14:01, 17:50 and 20:35 local time. The first two of these explosions

[3]A steep sided volcano built up alternating layers of lava and ash.

produced little ash but gas-rich plumes, whereas the final one was rich in both ash and gas. The plume was injected around 13-15 km (Waythomas et al., 2010; Karagulian et al., 2010), or as Prejean and Brodsky (2011) report, 12.5 ± 4 km, and according to data retrieved from IASI by Karagulian et al. (2010), released 1.7 Tg $SO_2$ into the atmosphere, the largest single injection since the eruption of Hudson in Chile in 1991, though other satellite measurements report $SO_2$ loadings ranging from 1.2 Tg from AIRS, to 1.5 Tg from OMI, to 2.2 Tg from GOME-2 (Karagulian et al. (2010) and references therein). For the 16 hours following the third injection, Kasatochi saw a continuous emission of ash.

### 4.3.1 Particular Parameters

The particular parameters used for the following analysis were:

- Volcano position: 52.177°N 175.508°W
- $SO_2$ retrieved from IASI passes from 7th - 16th August 2008, trajectories were generated from 4th - 16th
- Trajectories start every hour, from 00:00 - 23:00
- Trajectories generated at altitudes of 7500, 10000, 12000, 14000, 16000 m
- Calculated altitudes interpolated at every 500 m from 7.5-15 km

The altitude grid was chosen by looking at Carboni et al. (2016) which uses the same IASI retrieval and output files (figure 4.6). The extent of the generated trajectories was chosen to cover the majority of the retrieved plume heights when there was a red triangle present, representing a plume connected to the volcano, on the assumption that the plume would not have changed altitude dramatically in the time IASI was not observing. Trajectories were therefore generated across the main extent of the plume.

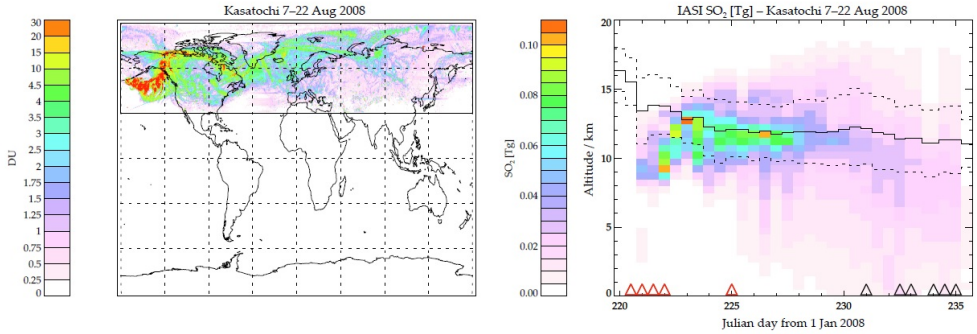


**Figure 4.6:** On the left is a map of the maximum $SO_2$ retrieved, within the considered region (black rectangle). On the right, a vertical distribution of the $SO_2$, with the colour bar representing the total mass, and each column representing a different IASI pass, every 12 hours. The black lines are the mean tropopause height, with the dotted lines representing the standard deviation from the mean, as calculated from the ECMWF profiles. The red triangles represent the presence of a new plume connected to the volcano, with the black triangles representing an old plume passing over the volcano (which may mask a new plume). Adapted from Carboni et al. (2016)

### 4.3.2 Discussion

The initial results of the analysis for the Kasatochi eruption are shown in figures 4.7, 4.8 and 4.9. In each of these plots, the columns represent a single air parcel, which evolves with time down the page. Therefore, what would be expected in the injection altitude case, figure 4.7, would be that every IASI pass shows the parcel injected at the same altitude, and so the column would be the same colour. The x axis, however, does not show every individual air parcel, but rather a time averaged representation: parcels are sorted into bins with respect to their injection time. It is therefore assumed that parcels injected at the same time should have approximately the same altitude. Due to the HYSPLIT trajectories only running for 72 hours, the horizontal lines representing the individual IASI passes will be the same length, resulting in the diagonal stripe across the plot.

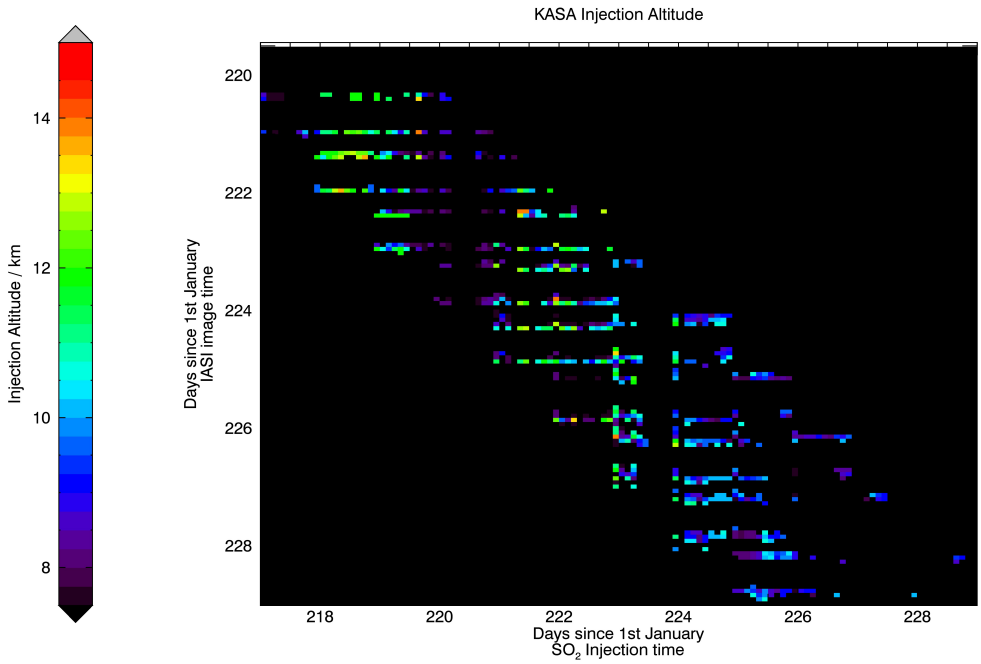


**Figure 4.7:** Distribution of plume injection altitudes over the Kasatochi eruption, taken as the starting points of the HYSPLIT trajectories

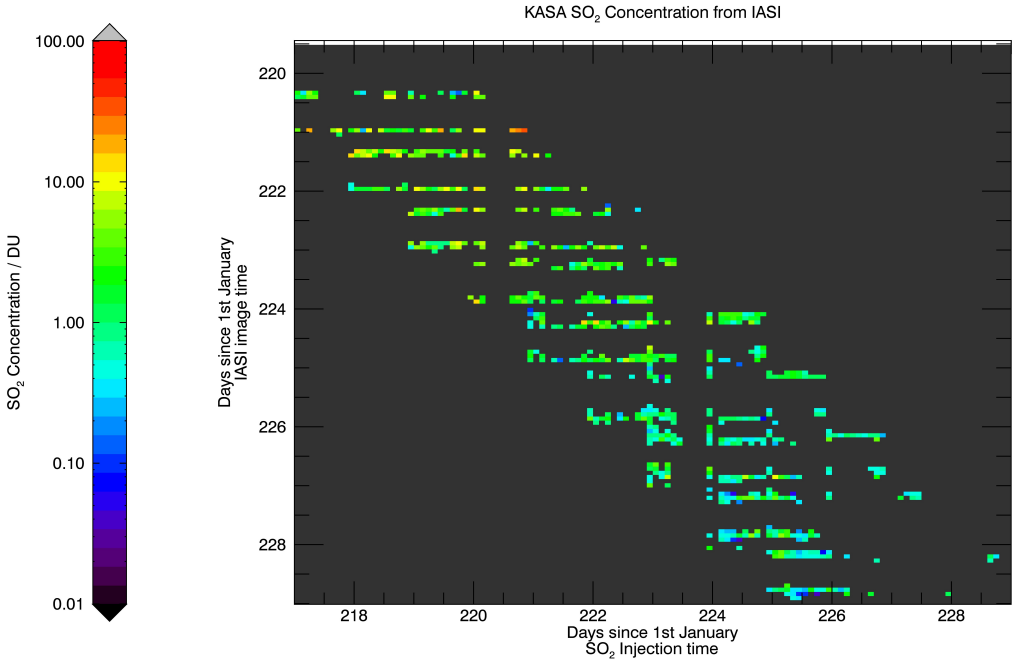


**Figure 4.8:** Distribution of $SO_2$ concentration over the Kasatochi eruption. Values for the concentration are taken from the associated IASI pixels

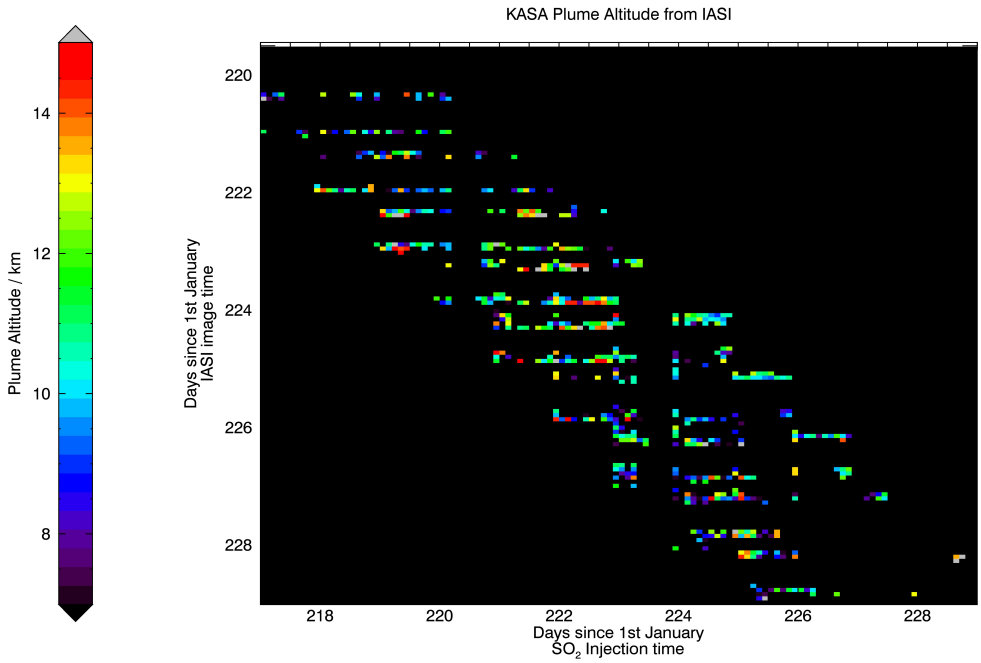


**Figure 4.9:** Distribution of plume height over the Kasatochi eruption. Values are taken from the associated IASI pixels

As can be see in figure 4.7, there is generally good agreement down the columns, with the exception of a few sections of late day 221. The figure implies injection altitudes for the most part of between 10 and 13 km, with the initial injection favouring the higher end of the range. This seems to agree with the values found in literature, with Prejean and Brodsky (2011) quoting 12.5 ± 4 km. As discussed in chapter 4, the local tropopause at the latitude of Kasatochi is approximately 11 km, meaning that anything green on the colourbar or higher will represent a stratospheric injection. Figure 4.9, plotted to the same colour scale, is difficult to interpret due to a spread in values, but it does seem to show a greater number of points around the 10-12 km level, confirming that a plume injected into the stratosphere tends not to cross the tropopause again.

The greatest success, however, comes from the $SO_2$ concentration plot. This clearly shows a decay down the columns from higher concentrations at the injection over the 72 hours covered, for each air parcel measured. When the columns are investigated individually, however, it is evident that the change in concentration down the columns is on the order of 10%, indicating that in this case, 72 hours

is not a long enough time frame to assess the $SO_2$ chemistry. The lifetime of $SO_2$ in the stratosphere is on the order of weeks (Wayne, 2000).

From the literature, it is apparent that the eruption of Kasatochi started on August 7th, or day 220, however the results show injections from day 218 onwards, the 5th. From the eyewitness accounts (Waythomas et al., 2010), it is clear that and injections on this date would have been recorded, especially one explosive enough to result in a reading at 13 km. On checking the IASI retrievals, no significant $SO_2$ was detected in the region on the days directly preceding the eruption. Barring any other large eruptions in the area, which according to records there were not (Cottrell, 2014), this means that the only remaining explanation is error in the system described here. Air parcels detected at a later date are being flagged as older parcels injected before. The 72 hours preceding an eruption are included in the analysis to allow for any degassing events before the main injection, but in this case they should be discounted. Interestingly, the number of points plotted over those days in comparable to that plotted in the days after the eruption, though the numbers making up the means (the individual blocks) are smaller than later.

A representation of the error in the algorithm is shown in figure 4.10. Here the mean of each column of the injection altitude plot (crosses) is shown, along with the standard deviation from that mean, shown by the red errorbars. The explosions detailed above occurred at 22:01, 01:50 and 04:35 (UTC)on the 7th and 8th, with the last one being the big injection of $SO_2$, the others mostly ash. If the results before the 7th, day 220, are discounted as already described, the majority of the means lie at or around the 10km altitude, with errors spread between 8 and 12. This overlaps with the values quoted in literature, though when viewed like this seems to underestimate, on average, especially those that quote the injection height at 18km. No trajectories were run at this altitude however, as this is around the top of the model's capabilities.

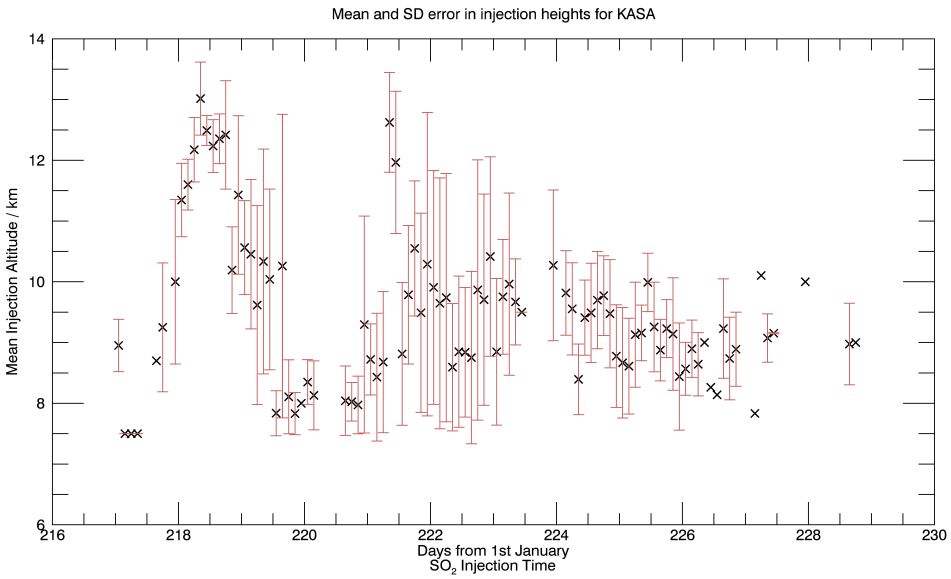


**Figure 4.10:** A plot of the error (standard deviation, red errorbars) in the mean of the plume injection altitude (black crosses).

In the main, the method described has successfully modelled the movement of a portion of the plume away from the volcano, with an associated error comparable to that found in other studies (for example, Prejean and Brodsky (2011)). It has been made apparent, however, that a facility should be included to be able to ignore trajectory final positions when they correspond to injection times before a certain point, but only in cases when it is certain that there was no eruption before a given day.

## 4.4 Sarychev Case Study

In contrast to Kasatochi, Sarychev, or Sarychev Peak, has a rather more active eruptive history, with confirmed historical eruptions dating back to the mid 1700s. Located in eastern Russia, Sarychev, another stratovolcano, is one of the most active volcanoes in the Kuril Islands, which extent from the Kamchatka Peninsula all the way south and west to the north Island of Japan.

Sarychev and the surrounding islands are remote and unmonitored, therefore there was no prior warning of the eruption. On the 11th June 2009, the first signs of

**Figure 4.11:** Image of the Sarychev eruption taken from the ISS, on the 12th of June
NASA Space Shuttle image, Image ISS020-E-9048, 2009

an eruption became evident in MODIS images: signs of thermal anomalies and weak degassing. By the 12th, this activity had intensified, and over the next 24 hours, at least eight explosive events were observed to send ash plumes to altitudes of 5–12 km and extended 350 km to the southeast (Rybin et al., 2011). There were also multiple pyroclastic flows along the northern flanks of the volcano, visible in figure 4.11. Several explosive events followed over the next four days, reaching altitudes of 4–11 km on 11–13 June and to 10–16 km on 15–16 June with a maximum of 20 km on 14th (Rybin et al., 2011), as reported by the Tokyo VAAC (Volcanic Ash Advisory Centres) (Jégou et al., 2013). Storms over the first day of the eruption resulted in heavy cloud cover, so satellite observation of the troposphere was obscured.

### 4.4.1 Particular Parameters

The particular parameters used for the following analysis were:

- Volcano position: 48.092°N 153.200°E
- $SO_2$ retrieved from IASI passes from 16th - 26th June 2009, trajectories were generated from 13th - 24th
- Trajectories start every hour, from 00:00 - 23:00
- Trajectories generated at altitudes of 7500, 10000, 12000, 14000 m

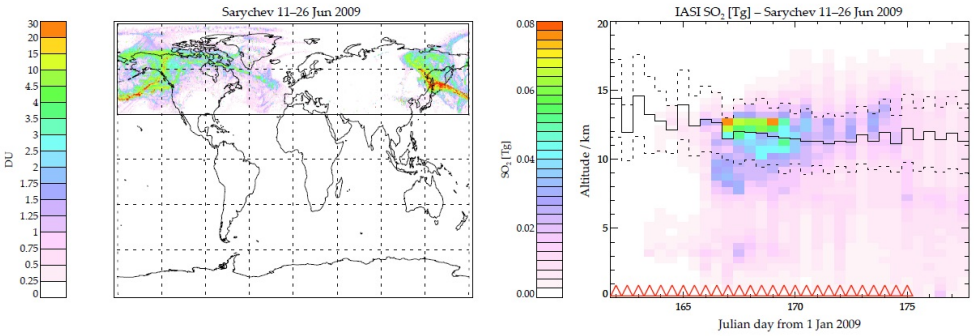


**Figure 4.12:** On the left is a map of the maximum $SO_2$ retrieved, within the considered region (black rectangle). On the right, a vertical distribution of the $SO_2$, with the colour bar representing the total mass, and each column representing a different IASI pass, every 12 hours. The black lines are the mean tropopause height, with the dotted lines representing the standard deviation from the mean, as calculated from the ECMWF profiles. The red triangles represent the presence of a new plume connected to the volcano. Adapted from Carboni et al. (2016)

- Calculated altitudes interpolated at every 500 m from 7.5-14 km

The altitude grid was chosen by looking at Carboni et al. (2016) which uses the same IASI retrieval and output files (figure 4.12), by the same method as the Kasatochi altitudes were chosen. The extent of the generated trajectories was chosen to cover the majority of the retrieved plume heights when there was a red triangle present, representing a plume connected to the volcano, on the assumption that the plume would not have changed altitude dramatically in the time IASI was not observing. Trajectories were therefore generated across the main extent of the plume, as reported in that study.

### 4.4.2 Discussion

The analysis of the injection height of the Sarychev eruption did not follow what was predicted as well as the Kasatochi eruption. For the first week of the analysis, there exists in figure 4.13 one or two orbits per day which show an anomalously high injection altitude.

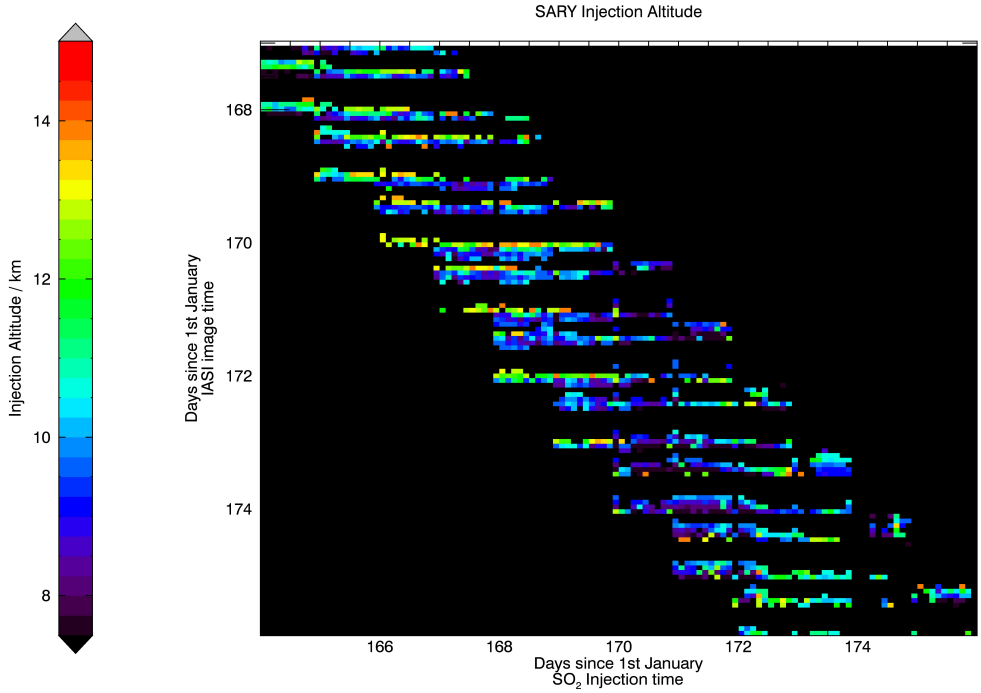


**Figure 4.13:** Distribution of plume injection altitudes over the Sarychev eruption, taken as the starting points of the HYSPLIT trajectories

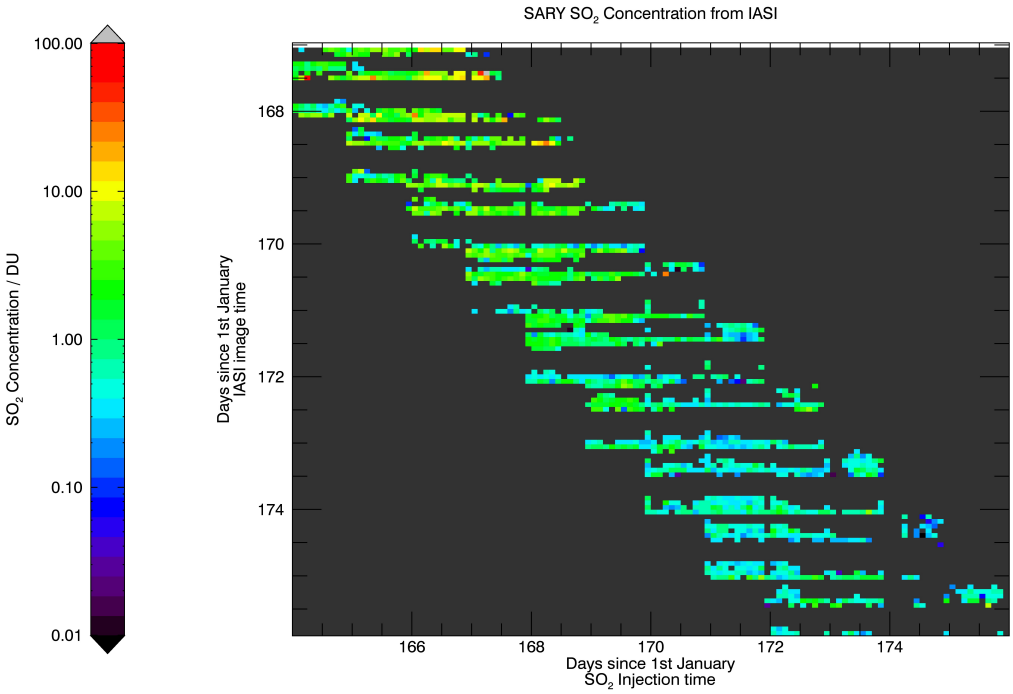


**Figure 4.14:** Distribution of $SO_2$ concentration over the Sarychev eruption. Values for the concentration are taken from the associated IASI pixels

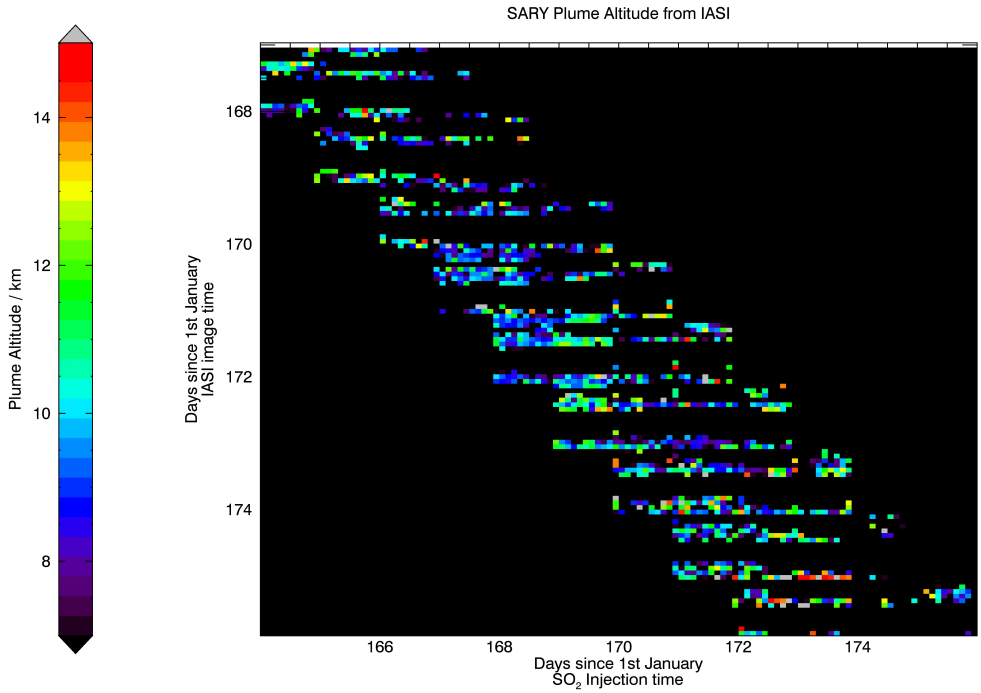


**Figure 4.15:** Distribution of plume height over the Sarychev eruption. Values are taken from the associated IASI pixels

As stated in section 4.3.2, a constant colour would be expected in individual columns of figure 4.13. For a large part of the figure, this is indeed the case, but during the first week of the eruption there appear anomalously high readings of the injection height, spread roughly 12 hours apart and corresponding to the ascending and descending IASI passes over the same geographical area. Looking at figure 4.12, however, it can be seen that altitude of the main part of the plume was measured at around 13 km, or yellow/orange on this colour scale, so it would do to not discount these entirely, especially as this is right at the height of the tropopause.

There are a number of possible explanations for these "stripes". It is always possible that there is some error in the algorithm procedure, though given the success of the Kasatochi analysis this seems unlikely. There is a small possibility of an error in the retrieval itself, though this error is unlikely to be something which is always present; the retrieval algorithm is 5 years old and something this apparent would have caused problems before now. There could be an issue, however, in either case, that crossing the international date line causes some problem with how the

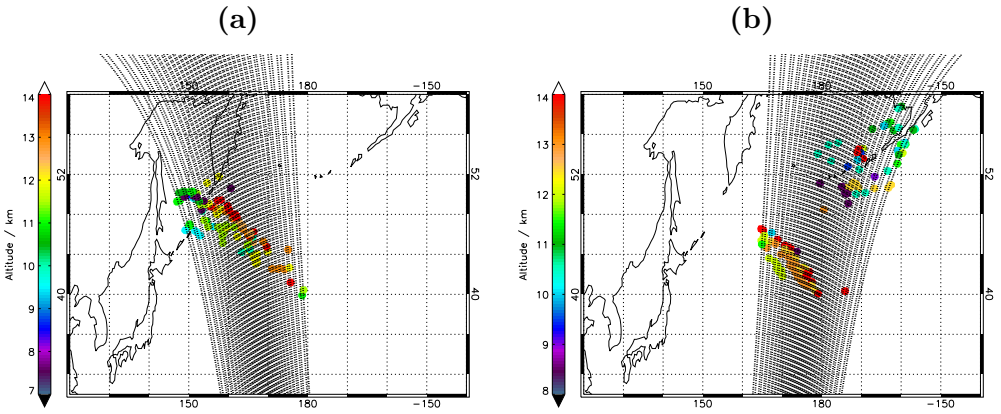


**Figure 4.16:** The IASI passes over the Sarychev region, on the 16th of June, which start at a) 0835 UTC and b) 2202 UTC. The colour bars represent the injection height retrieved from the trajectory analysis and the small black dots are the IASI pixels, plotted here to represent the path taken

time stamps are managed, though every care has been taken to prevent this. In fact, the trajectory algorithm was shifted to an alternative coordinate system, so that the longitude values did not jump from the -170s to +170s, however the anomalies persisted. The particular passes which have this problem are the same passes every day, and on both the ascending and descending tracks (see figures 4.16a and 4.16b).

This leaves one more possible explanation, and the one which seems the most likely: a meteorological explanation. The trajectory analysis of the eruption was run for IASI passes from the 16th of June onwards, but there were reports of activity from the 12th. This is due to there not being sufficient $SO_2$ concentrations to trigger the flag in the retrieval, and so no accurate measurements could be made until the 16th. It is possible that this $SO_2$, in the intervening few days, looped around to pass back over the volcano, where, in combination with the later plume, could be imaged. A different aged plume could cause the trajectory analysis to output a much higher injection height to account for the differences in input, and it does appear that figure 4.16b shows two separate plumes.

Looking at the plots of $SO_2$ concentration (figure 4.14) and plume altitude (figure 4.15), similar conclutions can be drawn to those in the Kasatochi study. The $SO_2$ concentrations follow a steady decay which is evident in the plot but too slow and over too short a time frame to be mathematically meaningful. The plume

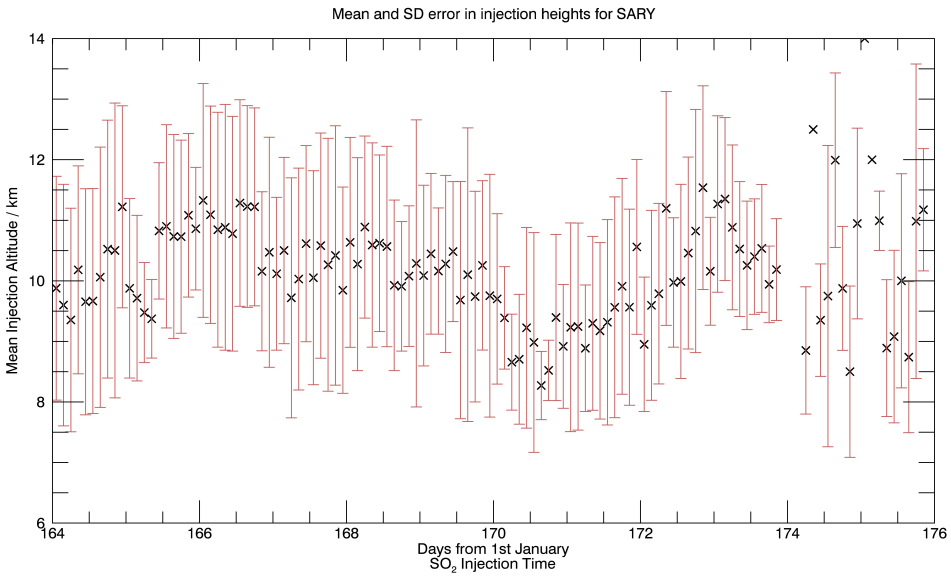


**Figure 4.17:** A plot of the error (standard deviation, red errorbars) in the mean of the plume injection altitude (black crosses).

altitude plot shows more coherence than the like plot for the Kasatochi eruption, with distinct patches of very similar colours. They are, for the most part, centred between 10 and 12 km which agrees with figure 4.12 as would be expected. This would seem to confirm that, although the trajectory analysis does not track every $SO_2$ parcel, that the selection that is tracked is representative of the whole.

Owing in part to the areas of high altitude injection, the error in this particular study is large, but perhaps not as large as might be expected (figure 4.17). As only 2 tracks were affected every 24 hours of the 72 analysed in each column, the anomalous values seem to be largely lost in the averages. The means are around 10 km, with a few sections closer to 12 km, and the errors fairly constant at around $\pm 2$ km, which is a similar order of magnitude to that found in the Kasatochi study.

The analysis here, and the plot produced in Carboni et al. (2016) (figure 4.12), would suggest that the eruption of Sarychev was not a stratospheric injection. Although there are portions of figure 4.13 that suggest an injection altitude of 13 km or higher, these are largely exceptions and are lost when averages are taken.

## 4.5 Overall Discussion and Conclusions

The final conclusions that can be drawn from the case studies discussed are as follows:

- The movement of the plume away from the volcano has been well described, for the most part, in both cases. The end points of the trajectories were only plotted if they fell within a radius of half a degree latitude or longitude from a pixel of $SO_2$ as measured by IASI, so the fact that a proportion of the plume was modelled is in itself a success.

- The error in both cases, as described by the standard deviation from the mean of the injection altitude for a particular column of the injection height plots (figures 4.7 and 4.13, with each column assumed to represent a single air parcel), is fairly constant at around $\pm 2$ km. In both cases this puts the mean values within error of the literature values, but both cases, for the most part, estimate an injection height lower than that quoted in literature.

- Although the plots of the $SO_2$ concentrations, figures 4.8 and 4.14, both show an encouraging downward trend, the time frame of this experiment was not long enough to measure a lifetime. The lifetime of atmospheric $SO_2$ is on the order of days to weeks, depending on the altitude, and the reduction in the first 72 hours is not significant enough to measure.

- In both cases, any drop in plume height due to dry deposition is also too slight to measure, if it is present at all. In the Kasatochi case, the plot of plume altitude (figure 4.9) appears too varied to draw any meaningful conclusions from.

The two case studies described here both had areas of success and of failure, but what has mostly been highlighted is the need for longer trajectories. The 72 hours generated by HYSPLIT is not long enough to observe any chemical phenomena, any dry deposition, or to draw any long term conclusions of plume transport. This, however, will always be a problem with forecast trajectories, if this method were to be

used in a forecast application such as that of volcanic advisory services for aviation: it is an error inherent to the trajectory model itself, that on time frames of 92 hours the error in position of the final point of the trajectory is so large it is on the order of the length of the trajectory itself, and in the absence of any more accurate method of predicting wind patterns and other meteorology, this problem will remain. If the method were to be restricted to the study of plume chemistry, for example, models of local meteorology as derived from measurements may provide a longer term insight, though interpolation between measurements would introduce its own errors.

Another limitation is the maximum altitude of the model. In a number of cases, trajectories were found to be truncated when the air parcel modelled was lofted above 18 km. Although these shorter trajectories may still be used in the analysis, up to the last point of the shorter trajectory, the parcel vanishing above a certain altitude is of course unphysical. Alternative meteorology may remedy this to an extent. There is also a chance for two trajectories to end in the same pixel. Were this to happen, some choice will have to me made as to the most appropriate starting altitude, or more likely, an mean of the two.

Through the Kasatochi case study, it has been made apparent that a facility should be included in the trajectory analysis algorithm to be able to ignore trajectory final positions when they correspond to injection times before a certain point, but that this should only apply when there is definite evidence for no eruption before a given time.

Overall, the principle of the trajectory analysis has been shown to be sound, and that in two separate cases it has been shown to model the movement of a plume away from a volcano well. It does, however, demonstrate that in its current, restricted, form, no quantifiable measurements of plume chemistry can be taken.

# 5
# Conclusions and Future Works

Here the general conclusions which can be drawn from this work are briefly outlined.

- Using the IASI retrievals to give an estimate of the volcanic contributions to the global $SO_2$ budget for both the stratosphere and the troposphere gave values for the stratosphere of the same order of magnitude as those found in the literature (figure 1.1), slightly higher due to the double counting inherent in the method. The value for the troposphere, on the other hand, is an order of magnitude lower than that estimated in figure 1.1, most likely due to the greatly reduced sensitivity of IASI when looking at the lower troposphere.

- Plotting these same IASI retrievals as yearly averages in terms of latitude appears to show a trend towards the larger eruptions occurring in the northern hemisphere, with the southern showing longer duration but lower $SO_2$ levels, though this could also be due to a greater proportion of volcanoes in the northern hemisphere. Although the $SO_2$ for each eruption is shown to cover a range of altitudes, some from ground level to the mid stratosphere, the volume mixing ratio generally peaks around the local level of the tropopause. This is unsurprising given that only explosive eruptions of significant magnitude were used in this analysis.

- The investigation into the combination of HYSPLIT model trajectories and IASI measurements as a method of determining plume movement, origin and chemistry was encouraging. The movement of the plume away from the volcano has been well described, for the most part, in both test cases, the August 2008 eruption of Kasatochi, and the June 2009 eruption of Sarychev. The error, as described by the standard deviation from the mean of the injection altitude for a particular column of the injection height plots (figures 4.7 and 4.13, with each column assumed to represent a single air parcel), is fairly constant at around $\pm 2$ km. In both cases this puts the mean values within error of the literature values, but both cases, for the most part, estimate an injection height lower than that quoted in literature. However, the time frame of the experiment is too short to measure any significant $SO_2$ chemistry, and changes in plume height over the same time frame are either too slight or absent entirely. Overall, the principle of the trajectory analysis has been shown to be sound, but demonstrates that currently no quantifiable measurements of plume chemistry can be taken.

A number of extensions to the presented works have become apparent over the course of the studies.

In order to increase the accuracy of the estimations of the stratospheric $SO_2$ loading due to volcanism, from IASI measurements, there are two main sources of error to be overcome: the latitudinal variation in the gap between IASI passes, causing areas of the plume to be missed; and the potential for double counting, counting the same parcel of $SO_2$ of subsequent days. To solve the former a scaling factor could be introduced. Although it would be relatively simple to estimate the number of pixels which would fit into the gap between passes and use this as a scaling factor, this would only give the maximum amount of plume that could be missed on each pass, though this would be a good first step. In fact, the proportion of plume missed will vary with every eruption, and with every day as the plume moves, so the best approach would likely be to use the interpolation procedure: as shown in figure 3.6, the plume on either side of the gap between tracks is compared

and a linear gradient between the two is assumed. The amount of space filled between the passes compared to the space occupied by the plume would give a fair estimation of the amount of $SO_2$ which was not counted, though assuming a fairly uniform distribution of $SO_2$ throughout the plume.

Solving the problem of the double counting presents more of a problem, whilst relatively simple for eruptions comprising a single injection, the process would still be relatively manual, and rely on the user being able to see in the image when the plume is no longer attached to the volcano. It could also be possible to track individual plumes day by day, comparing apparent new injections to other observations, ground based or other satellites. Although this could potentially be partially automated by the use of a trajectory model, this process still relies for the most part on what can manually be observed by the user. Although relying on user interaction, any removal of double counting can only increase the accuracy of the estimations.

In the case of the HYSPLIT studies, the basic principle has been shown to be sound. The first additional area to be investigated should be alternative meteorological datasets. The data used herein was chosen for the greater spacial resolution than the majority of the alternatives, with only a small increase in the calculation time, but further investigation should be given to the difference in the overall outcomes from using other meteorology.

From the investigation into the Kasatochi eruption, it became clear that in some cases the method was selecting trajectories which began before the first eruption was registered. It is still important to include these trajectories in case of eruptions from unmonitored volcanoes, if there was any degassing before the first explosive eruption, and to account for any external sulphur sources, but a facility should be built into the procedure to discount these trajectories if the eruption is well documented and initially explosive.

The treatment of the model output is obviously specific to the data format outputted by the HYSPLIT model. However, it would be useful to be able to generalise the data format so that the procedure could be applied to other models. This would mean an extra level of processing, with presumably a keyword for the

particular model, which would input the generated datafile and output the data in a generalised format. This may also reduce a problem some of the analysis had, with the HYSPLIT trajectories initiated at too high an altitude being cut off at the top of the model. In these cases the entirety of that trajectory was discounted, as the procedure could not manage trajectories which were not of a uniform length. Feasibly any trajectory shorter than expected could be compared line-by-line with one which it is required to be interpolated, as long as they both reach the required length to cover the end time, but this would make an already relatively slow running procedure take orders of magnitude longer.

The biggest area of further study arising from the HYSPLIT chapter, however, is the need to apply the method to other eruptions. The differences between just the two eruptions reported are significant enough to investigate any trends caused by such factors as the differences in latitude, the presence and concentration of volcanic ash and the effect it has on plume chemistry, the differences in vertical wind fields and the presence of other meteorology such as rainfall.

In conclusion, the questions addressed at the end of chapter 1 have been investigated using pre-existing IASI retrievals. The mass of $SO_2$ in the troposphere and the stratosphere due to volcanic eruptions was calculated by scaling the IASI retrievals against the height of the tropopause, and found to be on par with values found in literature, but with significant error terms. Global averages of sulphur dioxide loading were also presented. Finally, it has been shown that, in principle, HYSPLIT and other trajectory models can be used in conjunction with IASI to determine an injection altitude for particular eruptions. For both test cases, however, the altitude predicted was fractionally lower than that presented in literature, and the length of the trajectories was not sufficient to study the plume chemistry, prompting further investigation.

# Appendices

# A

# Converting Pressure to Altitude

Atmospheric pressure can be converted to altitude, assuming a standard atmosphere, as follows.

The Hydrostatic equation (equation A.1) can be combined with the Ideal Gas Law (A.2):

$$\frac{dP}{dz} = -\rho g \tag{A.1}$$

$$P = \rho RT \tag{A.2}$$

The density term, $\rho$, can be eliminated and we are left with:

$$\frac{dP}{dz} = -\frac{g}{RT}P \tag{A.3}$$

If equation A.3 were to be solved for constant $T$ and $g$, the Hypsometric equation for the variation of pressure with altitude would be derived, but this assumes a zero Lapse rate, which is not very physical. Therefore, at least the temperature must be assumed to vary with $z$ (in fact the gravity term does as well but the change is negligible so it is generally taken as a constant).

$$\frac{dP}{dz}[z] = -\frac{g}{RT[z]}P[z] \tag{A.4}$$

Which can then be integrated with respect to altitude.

$$P[z] = P_0 EXP\left[-\frac{g}{R}\left(\int_0^z \frac{1}{T[x]}\,dx\right)\right] \tag{A.5}$$

Where $x$ is just a filler variable for the integration procedure.

The temperature varies with height with the Lapse Rate $L$ from an initial temperature at zero altitude, $T_0$. If this is substituted, the integral term from equation A.5 can be reduced.

$$\int_0^z \frac{dx}{T_0 + Lx} == \frac{1}{L}\Big[\ln(T_0 + Lz) - \ln(T_0)\Big] \tag{A.6}$$

$$P[z] = P_0 EXP\Big\{-\frac{g}{RL}\Big[\ln(T_0 + Lz) - \ln(T_0)\Big]\Big\} \tag{A.7}$$

$$-\frac{RL}{g}\Big[\ln\Big(\frac{P}{P_0}\Big)\Big] = \ln\Big(\frac{T_0 + Lz}{T_0}\Big) \tag{A.8}$$

And leaving us with the final expression:

$$z = \frac{T_0}{L}\Big[\Big(\frac{P}{P_0}\Big)^{-\frac{RL}{g}} - 1\Big] \tag{A.9}$$

For a standard atmosphere, the following constants can be used:

$P_0$ - The atmospheric pressure at zero altitude - 101325 Pa

$T_0$ - The atmospheric temperature at zero altitude - 288.15 K

$g$ - The acceleration due to gravity - 9.80665 $\text{ms}^{-1}$

$L$ - The lapse rate - $-6.5 \times 10^{-3}$ $\text{Km}^{-1}$

$R$ - Gas constant for air - 287.053 $\text{Jkg}^{-1}\text{K}^{-1}$

Substituting in for these values, we are left with the simplified form:

$$z = 44330.8 - 4946.54 \times P(Pa)^{0.1902632} \tag{A.10}$$

# Bibliography


Adame, J., Valentí – Pía, M., and Gil-Ojeda, M. (2015). Impact evaluation of potential volcanic plumes over Spain. *Atmospheric Research*, 160:39–49.

Andres, R. J. and Kasgnoc, A. D. (1998). A time-averaged inventory of subaerial volcanic sulfur emissions. *Journal of Geophysical Research: Atmospheres*, 103:25251–61.

Badr, O. and Probert, S. D. (1994). Atmospheric Sulphur: Trends, Sources, Sinks and Environmental Impacts. *Applied Energy*, 47:1–67.

Bey, I., Jacob, D., Yantosca, R., Logan, J., Field, B., Fiore, A., Li, Q., Liu, H., Mickley, L., and Schultz, M. (2001). Global modeling of tropospheric chemistry with assimilated meteorology: Model description and evaluation. *Journal of Geophysical Research: Atmospheres*, 106(D19):23073–23095.

Blumstein, D., Chalon, G., Carlier, T., Buil, C., Hébert, P., Maciaszek, T., Ponce, G., Phulpin, T., Tournier, B., Simeoni, D., Astruc, P., Clauss, A., Kayal, G., and Jegou, R. (2004). IASI instrument: Technical description and measured performances. *European Space Agency, (Special Publication) ESA SP*, 5543:49–56.

Bluth, G. J. S., Schnetzler, C. C., Krueger, A. J., and Walter, L. S. (1993). The contribution of explosive volcanism to global atmospheric sulphur dioxide concentrations. *Nature*, 366(6453):327–329.

Boichu, M., Clarisse, L., Péré, J.-C., Herbin, H., Goloub, P., Thieuleux, F., Ducos, F., Clerbaux, C., and Tanré, D. (2015). Temporal variations of flux and altitude of sulfur dioxide emissions during volcanic eruptions: implications for long-range dispersal of volcanic clouds. *Atmospheric Chemistry and Physics*, 15(14):8381–8400.

Brenot, H., Theys, N., Clarisse, L., van Geffen, J., van Gent, J., Van Roozendael, M., van der A, R., Hurtmans, D., Coheur, P.-F., Clerbaux, C., Valks, P., Hedelt, P., Prata, F., Rasson, O., Sievers, K., and Zehner, C. (2014). Support to Aviation Control Service (SACS): an online service for near-real-time satellite monitoring of volcanic plumes. *Natural Hazards and Earth System Science*, 14(5):1099–1123.

Bursik, M., Kobs, S., Burns, A., Braitseva, O., Bazanova, L., Melekestsev, I., Kurbatov, A., and Pieri, D. (2009). Volcanic plumes and wind: Jetstream interaction examples and implications for air traffic. *Journal of Volcanology and Geothermal Research*, 186(1):60–67.

Carboni, E., Grainger, R., Walker, J., Dudhia, A., and Siddans, R. (2012). A new scheme for sulphur dioxide retrieval from IASI measurements: application to the Eyjafjallajökull eruption of April and May 2010. *Atmospheric Chemistry and Physics*, 12(23):11417–11434.

Carboni, E., Grainger, R. G., Mather, T. A., Pyle, D. M., Thomas, G. E., Siddans, R., Smith, A. J. A., Dudhia, A., Koukouli, M. E., and Balis, D. (2016). The vertical distribution of volcanic SO2 plumes measured by IASI. *Atmospheric Chemistry and Physics*, 16(7):4343–4367.

Carn, S., Krotkov, N., Yang, K., and Krueger, A. J. (2013). Measuring global volcanic degassing with the Ozone Monitoring Instrument (OMI). *Geological Society, London, Special Publications*, 380:229–257.

Carn, S. A., Krotkov, N. A., Yang, K., Hoff, R. M., Prata, A. J., Krueger, A. J., Loughlin, S. C., and Levelt, P. F. (2007). Extended observations of volcanic SO2 and sulfate aerosol in the stratosphere. *Atmospheric Chemistry and Physics Discussions*, 7(1):2857–2871.

Carn, S. A., Krueger, A. J., Arellano, S., Krotkov, N. A., and Yang, K. (2008). Daily monitoring of Ecuadorian volcanic degassing from space. *Journal of Volcanology and Geothermal Research*, 176(1):141–150.

Carn, S. A., Strow, L. L., de Souza-Machado, S., Edmonds, Y., and Hannon, S. (2005). Quantifying tropospheric volcanic emissions with AIRS: The 2002 eruption of Mt. Etna (Italy). *Geophysical Research Letters*, 32(2):1–5.

Carn, S. A., Yang, K., Prata, A. J., and Krotkov, N. A. (2015). Extending the long-term record of volcanic SO2 emissions with the Ozone Mapping and Profiler Suite nadir mapper. *Geophysical Research Letters*, 42(3):925–932.

Charlson, R. J., Schwartz, S. E., Hales, J. M., Cess, R. D., Coakley, J. A., Hansen, J. E., and Hofmann, D. J. (1992). Climate Forcing by Anthropogenic Aerosols. *Science*, 255(5043):423 – 430.

Chin, M. and Davis, D. D. (1993). Global sources and sinks of OCS and CS2 and their distributions. *Global Biogeochemical Cycles*, 7(2):321–337.

Chin, M. and Davis, D. D. (1995). A reanalysis of carbonyl sulfide as a source of stratospheric background sulfur aerosol. *Journal of Geophysical Research*, 100(D5):8993.

Chin, M., Rood, R. B., Lin, S.-J., Muller, J.-F., and Thompson, A. M. (2000). Atmospheric sulfur cycle simulated in the global model GOCART: Model description and global properties. *Journal of Geophysical Research*, 105:24671–24687.

Clarisse, L., Coheur, P. F., Theys, N., Hurtmans, D., and Clerbaux, C. (2014). The 2011 Nabro eruption, a SO2 plume height analysis using IASI measurements. *Atmospheric Chemistry and Physics*, 14:3095–3111.

Clarisse, L., Hurtmans, D., Prata, A. J., Karagulian, F., Clerbaux, C., De Mazière, M., and Coheur, P.-F. (2010). Retrieving radius, concentration, optical depth, and mass of different types of aerosols from high-resolution infrared nadir spectra. *Applied optics*, 49(19):3713–3722.

Clerbaux, C., Boynard, a., Clarisse, L., George, M., Hadji-Lazaro, J., Herbin, H., Hurtmans, D., Pommier, M., Razavi, a., Turquety, S., Wespes, C., and Coheur, P.-F. (2009). Monitoring of atmospheric composition using the thermal infrared IASI/MetOp sounder. *Atmospheric Chemistry and Physics*, 9(16):6041–6054.

Cottrell, L. (2014). Smithsonian Institute - Global Volcanism Program.

Draxler, R. R. and Hess, G. D. (1998). An Overview of the HYSPLIT_4 Modelling System for Trajectories, Dispersion, and Deposition. *Australian Meteorological Magazine*, 47(June 1997):295–308.

Draxler, R. R. and Taylor, A. D. (1982). Horizontal Dispersion Parameters for Long-Range Transport Modeling. *Journal of Applied Meteorology*, 21(3):367–372.

Eckhardt, S., Prata, A. J., Seibert, P., Stebel, K., and Stohl, A. (2008). Estimation of the vertical profile of sulfur dioxide injection into the atmosphere by a volcanic eruption using satellite column measurements and inverse transport modeling. *Atmospheric Chemistry and Physics*, 8:3881–3897.

Eisinger, M. and Burrows, J. P. (1998). Tropospheric sulfur dioxide observed by the ERS-2 GOME instrument. *Geophysical Research Letters*, 25(22):4177.

Eyring, V., Isaksen, I. S. A., Berntsen, T., Collins, W. J., Corbett, J. J., Endresen, O., Grainger, R. G., Moldanova, J., Schlager, H., and Stevenson, D. S. (2010). Transport impacts on atmosphere and climate: Shipping. *Atmospheric Environment*, 44(37):4735–4771.

Fioletov, V. E., McLinden, C. A., Krotkov, N., Moran, M. D., and Yang, K. (2011). Estimation of SO2 emissions using OMI retrievals. *Geophysical Research Letters*, 38(21).

Fromm, M., Kablick III, G., Nedoluha, G., Carboni, E., Grainger, R., Campbell, J., and Lewis, J. (2014). Correcting the record of volcanic stratospheric aerosol impact : Nabro and Sarychev Peak. *Journal of Geophysical Research: Atmospheres*, 119(7):343–364.

Graf, H.-F., Feichter, J., and Langmann, B. (1997). Volcanic sulfur emissions: Estimates of source strength and its contribution to the global sulfate distribution. *Journal of Geophysical Research: Atmospheres*, 102(D9):10727–10738.

Jacobson, M. Z. (2005). *Fundamentals of Atmospheric Modeling*. Cambridge University Press, 2nd edition.

Jégou, F., Berthet, G., Brogniez, C., Renard, J.-B., François, P., Haywood, J. M., Jones, A., Bourgeois, Q., Lurton, T., Auriol, F., Godin-Beekmann, S., Guimbaud, C., Krysztofiak, G., Gaubicher, B., Chartier, M., Clarisse, L., Clerbaux, C., Balois, J. Y., Verwaerde, C., and Daugeron, D. (2013). Stratospheric aerosols from the Sarychev volcano eruption in the 2009 Arctic summer. *Atmospheric Chemistry and Physics*, 13(13):6533–6552.

Karagulian, F., Clarisse, L., Clerbaux, C., Prata, A. J., Hurtmans, D., and Coheur, P. F. (2010). Detection of volcanic SO2 , ash, and H2SO4 using the Infrared Atmospheric Sounding Interferometer (IASI). *Journal of Geophysical Research*, 115:D00L02.

Koch, D., Jacob, D., Tegen, I., Rind, D., and Chin, M. (1999). Tropospheric sulfur simulation and sulfate direct radiative forcing in the Goddard Institute for Space Studies general circulation model. *Journal of Geophysical Research*, 104(D19):23799.

Kristiansen, N. I., Stohl, A., Prata, A. J., Richter, A., Eckhardt, S., Seibert, P., Hoffmann, A., Ritter, C., Bitar, L., Duck, T. J., and Stebel, K. (2010). Remote sensing and inverse transport modeling of the Kasatochi eruption sulfur dioxide cloud. *Journal of Geophysical Research*, 115.

Mather, T., Pyle, D., and Heaton, T. (2008). Investigation of the use of filter packs to measure the sulphur isotopic composition of volcanic sulphur dioxide and the sulphur and oxygen isotopic composition of volcanic sulphate aerosol. *Atmospheric Environment*, 42(19):4611–4618.

Mather, T. A., Pyle, D. M., and Oppenheimer, C. (2013). Tropospheric Volcanic Aerosol. In *Volcanism and the Earth's Atmosphere*, pages 189–212. American Geophysical Union.

McCormick, B. T., Edmonds, M., Mather, T. A., Campion, R., Hayer, C. S. L., Thomas, H. E., and Carn, S. A. (2013). Volcano monitoring applications of the Ozone Monitoring Instrument. *Geol. Soc. Lond.*, 380(1):259–291.

McQueen, J. T. and Draxler, R. R. (1994). Evaluation of model back trajectories of the Kuwait oil fires smoke plume using digital satellite data. *Atmospheric Environment*, 28(13):2159–2174.

Montzka, S. A., Calvert, P., Hall, B. D., Elkins, J. W., Conway, T. J., Tans, P. P., and Sweeney, C. (2007). On the global distribution, seasonality, and budget of atmospheric carbonyl sulfide (COS) and some similarities to CO2. *Journal of Geophysical Research*, 112(D9):D09302.

Moran, S. C., Newhall, C., and Roman, D. C. (2011). Failed magmatic eruptions: Late-stage cessation of magma ascent. *Bulletin of Volcanology*, 73(2):115–122.

Oberhuber, J. M., Herzog, M., Graf, H.-F., and Schwanke, K. (1998). Volcanic plume simulation on large scales. *Journal of Volcanology and Geothermal Research*, 87(1):29–53.

Oppenheimer, C., Scaillet, B., and Martin, R. S. (2011). Sulfur degassing from volcanoes: source conditions, surveillance, plume chemistry and earth system impacts. *Reviews in Mineralogy & Geochemistry*, 73:363–421.

Penner, J. E., Hegg, D., and Leaitch, R. (2001). Unraveling the role of aerosols in climate change. *Environmental Science & Technology*, 35(15):332A–340A.

Prata, A. J., Barton, I. J., Johnson, R. W., Kamo, K., and Kingwell, J. (1991). Hazard from volcanic ash. *Nature*, 354(6348):25.

Prata, A. J. and Kerkmann, J. (2007). Simultaneous retrieval of volcanic ash and SO2 using MSG-SEVIRI measurements. *Geophysical Research Letters*, 34(5).

Prejean, S. G. and Brodsky, E. E. (2011). Volcanic plume height measured by seismic waves based on a mechanical model. *Journal of Geophysical Research*, 116(B1):B01306.

Prentiss, D. (2015). Museums Teaching Planet Earth.

Preston, J. (2015). *Application of the Infrared Atmospheric Sounding Interferometer to Arc-Scale Monitoring of Volcanic SO2*. PhD thesis.

Ramachandran, S., Ramaswamy, V., Stenchikov, G. L., and Robock, A. (2000). Radiative impact of the Mount Pinatubo volcanic eruption: Lower stratospheric response. *Journal of Geophysical Research*, 105:24409.

Read, W. G., Froidevaux, L., and Waters, J. W. (1993). Microwave limb sounder measurement of stratospheric SO2 from the Mt. Pinatubo Volcano. *Geophysical Research Letters*, 20(12):1299–1302.

Rex, M., Wohltmann, I., Ridder, T., Lehmann, R., Rosenlof, K., Wennberg, P., Weisenstein, D., Notholt, J., Krüger, K., Mohr, V., and Tegtmeier, S. (2014). A tropical West Pacific OH minimum and implications for stratospheric composition. *Atmospheric Chemistry and Physics*, 14(9):4827–4841.

Robock, A. (2000). Volcanic eruptions and climate. *Reviews of Geophysics*, 38(2):191–219.

Rogers, C. D. (2000). *Inverse Methods for Atmospheric Sounding: Theory and Practice*. World Scientific.

Rolph, G. D. and Draxler, R. R. (1990). Sensitivity of Three-Dimensional Trajectories to the Spatial and Temporal Densities of the Wind Field. *Journal of Applied Meteorology*, 29(10):1043–1054.

Rotstayn, L. D. and Lohmann, U. (2002). Simulation of the tropospheric sulfur cycle in a global model with a physically based cloud scheme. *Journal of Geophysical Research: Atmospheres*, 107(21).

Rybin, A., Chibisova, M., Webley, P., Steensen, T., Izbekov, P., Neal, C., and Realmuto, V. (2011). Satellite and ground observations of the June 2009 eruption of Sarychev Peak volcano, Matua Island, Central Kuriles. *Bulletin of Volcanology*, 73(9):1377–1392.

Sander, S. P., Friedl, R. R., Golden, D. M., Kurylo, M. J., Huie, R. E., Orkin, V. L., Moortgat, G. K., Ravishankara, A. R., Kolb, C. E., and Molina, M. J. (2003). Chemical Kinetics and Photochemical Data for Use in Atmospheric Studies - Part 4. Technical Report 14.

Schmidt, A., Carslaw, K. S., Mann, G. W., Rap, A., Pringle, K. J., Spracklen, D. V., Wilson, M., and Forster, P. M. (2012). Importance of tropospheric volcanic aerosol for indirect radiative forcing of climate. *Atmospheric Chemistry and Physics*, 12(16):7321–7339.

Schoeberl, M. R., Doiron, S., Lait, L. R., Newman, P. A., and Krueger, A. J. (1993). A simulation of the Cerro Hudson SO2 Cloud. *Journal of Geophysical Research*, 98(D2):2949.

Schumann, U., Weinzierl, B., Reitebuch, O., Schlager, H., Minikin, A., Forster, C., Baumann, R., Sailer, T., Graf, K., Mannstein, H., Voigt, C., Rahm, S., Simmet, R., Scheibe, M., Lichtenstern, M., Stock, P., R??ba, H., Sc???auble, D., Tafferner, A., Rautenhaus, M., Gerz, T., Ziereis, H., Krautstrunk, M., Mallaun, C., Gayet, J. F., Lieke, K., Kandler, K., Ebert, M., Weinbruch, S., Stohl, A., Gasteiger, J., Gro, S., Freudenthaler, V., Wiegner, M., Ansmann, A., Tesche, M., Olafsson, H., and Sturm, K. (2011). Airborne observations of the Eyjafjalla volcano ash cloud over Europe during air space closure in April and May 2010. *Atmospheric Chemistry and Physics*, 11(5):2245–2279.

Searcy, C., Dean, K., and Stringer, W. (1998). PUFF: A high-resolution volcanic ash tracking model. *Journal of Volcanology and Geothermal Research*, 80(1-2):1–16.

Sheng, J.-X., Weisenstein, D. K., Luo, B., Rozanov, E., Stenke, A., Anet, J., Bingemer, H., and Peter, T. (2014). Global atmospheric sulfur budget under volcanically quiescent conditions: Aerosol-chemistry-climate model predictions and validation. *Journal of Geophysical Research : Atmospheres*, 120(1):256–276.

Sheng, J.-X., Weisenstein, D. K., Luo, B.-P., Rozanov, E., Stenke, A., Anet, J., Bingemer, H., and Peter, T. (2015). Global atmospheric sulfur budget under volcanically quiescent conditions: Aerosol-chemistry-climate model predictions and validation. *Journal of Geophysical Research: Atmospheres*, 120(1):256–276.

Soucy, M.-A., Châteauneuf, F., Giroux, J., and Roy, C. (2006). Looking at the air from space: FTIR atmospheric sounding applications for remote sensing satellites. *Special Report Instrumentation & Analytics, ABB Review*, pages 50–3.

Sparks, R. S. J., Biggs, J., and Neuberg, J. W. (2012). Monitoring Volcanoes. *Science*, 335(6074):1310–1311.

Stein, A. F., Draxler, R. R., Rolph, G. D., Stunder, B. J. B., Cohen, M. D., and Ngan, F. (2015). NOAA's HYSPLIT Atmospheric Transport and Dispersion Modeling System. *Bulletin of the American Meteorological Society*, 96(12):2059–2077.

Stevenson, D. S., Johnson, C. E., Collins, W. J., and Derwent, R. G. (2003). The Tropospheric Sulphur Cycle and the role of Volcanic SO2. *Geological Society, London, Special Publications*, Volcanic D(213):295–305.

Stohl, A., Hittenberger, M., and Wotawa, G. (1998). Validation of the lagrangian particle dispersion model FLEXPART against large-scale tracer experiment data. *Atmospheric Environment*, 32(24):4245–4264.

Symonds, R. B., Gerlach, T. M., and Reed, M. H. (2001). Magmatic gas scrubbing: Implications for volcano monitoring. *Journal of Volcanology and Geothermal Research*, 108(1-4):303–341.

Tanaka, H. (1994). Development of a prediction scheme for volcanic ash fall from Redoubt Volcano, Alaska. In *Volcanic ash and aviation safety; proceedings of the first international symposium on volcanic ash and aviation safety: U.S. Geological Survey Bulletin 2047*, pages 283–291.

Thomason, L. and Peter, T. (2006). Assessment of stratospheric aerosol properties (ASAP). *SPARC Report*, (4):348.

Twomey, S. (1977). Influence of polution on the shortwave albedo of clouds. *Journal of the Atmospheric Sciences*, 34(7):1149–1152.

Venzke, E. e. (2013). Global Volcanism Program, Volcanoes of the World v. 4.5.0.

Vernier, J. P., Thomason, L. W., Pommereau, J. P., Bourassa, A., Pelon, J., Garnier, A., Hauchecorne, A., Blanot, L., Trepte, C., Degenstein, D., and Vargas, F. (2011). Major influence of tropical volcanic eruptions on the stratospheric aerosol layer during the last decade. *Geophysical Research Letters*, 38(12):1–8.

Wayne, R. P. (2000). *Chemistry of Atmospheres*. Oxford University Press, 3rd edition.

Waythomas, C. F., Scott, W. E., Prejean, S. G., Schneider, D. J., Izbekov, P., and Nye, C. J. (2010). The 7–8 August 2008 eruption of Kasatochi Volcano, central Aleutian Islands, Alaska. *Journal of Geophysical Research*, 115:B00B06.

Werner, C. A., Doukas, M. P., and Kelly, P. J. (2011). Gas emissions from failed and actual eruptions from Cook Inlet Volcanoes, Alaska, 1989-2006. *Bulletin of Volcanology*, 73(2):155–173.

WMO (1957). Definition of the thermal tropopause. *WMO Bull.*, 6(136).

Woodhouse, M. J., Hogg, A. J., and Phillips, J. C. (2016). A global sensitivity analysis of the PlumeRise model of volcanic plumes. *Journal of Volcanology and Geothermal Research*.

Woodhouse, M. J., Hogg, A. J., Phillips, J. C., and Sparks, R. S. J. (2013). Interaction between volcanic plumes and wind during the 2010 Eyjafjallajökull eruption, Iceland. *Journal of Geophysical Research: Solid Earth*, 118(1):92–109.

Yang, K., Dickerson, R. R., Carn, S. A., Ge, C., and Wang, J. (2013). First observations of SO2 from the satellite Suomi NPP OMPS: Widespread air pollution events over China. *Geophysical Research Letters*, 40(18):4957–4962.

Yang, K., Liu, X., Krotkov, N. A., Krueger, A. J., and Carn, S. A. (2009). Estimating the altitude of volcanic sulfur dioxide plumes from space borne hyper-spectral UV measurements. *Geophysical Research Letters*, 36:1–6.